Thesis for the degree of Licentiate of Engineering

# Nonlinear Dynamics of Frequency Sweeping Energetic Particle Modes in Tokamaks

**Frida Eriksson**


CHALMERS

Department of Earth and Space Sciences
Chalmers University of Technology
Göteborg, Sweden 2016

Nonlinear Dynamics of Frequency Sweeping Energetic Particle Modes in Tokamaks
FRIDA ERIKSSON



Technical Report 45L

Department of Earth and Space Sciences
Plasma Physics and Fusion Energy
Chalmers University of Technology
SE-412 96 Göteborg, Sweden
Telephone +46 (0)31-772 1000

Chalmers Reproservice
Göteborg, Sweden 2016

# Nonlinear Dynamics of Frequency Sweeping Energetic Particle Modes in Tokamaks

Frida Eriksson
Department of Earth and Space Sciences
Chalmers University of Technology
SE-412 96 Göteborg, Sweden

**Abstract**

In a burning plasma, such as the next generation tokamak experiment ITER, significant numbers of highly energetic particles will be produced via nuclear reactions. The presence of energetic particles, be it fusion born alpha particles or ions accelerated by auxiliary heating schemes, may excite kinetic instabilities and thereby affect the heating and transport of all particles in the plasma. Of particular interest is the toroidal Alfvén eigenmode (TAE), a cavity mode that can be excited by super Alfvénic ions as they slow down due to friction-like collisions with the background plasma and eventually hit the wave-particle resonances. Such modes have attracted much attention during almost 30 years, since their detection provides diagnostic opportunities to probe the plasma core. However, their presence and long-term behavior are still far from understood. They may have detrimental effects on the plasma confinement and heating, but can potentially also be utilized as a collisionless way to channel power from the fast ions to the bulk plasma.

In this thesis we employ linear and nonlinear analysis to study fast particle driven TAEs whose signals exhibit frequency sweeping. Their existence is tied to the formation and evolution of phase space structures known as holes and clumps in the non-thermal fast particle distribution. A one-dimensional "bump-on-tail" model is employed and used to investigate the stability of a phase space plateau that emerges early in the mode evolution cycle. Fast particle collisions and sources are included in the analysis in order to substantiate the role of the plateau as a hole/clump breeding ground from which the frequency sweeping initiates. Furthermore, the ideas of phase-locking of fast ions orbits in the wave-particle resonances is used to calculate the radial motion of already established hole/clump modes during the frequency sweeping for the ideal cases of deeply trapped and well passing particles, and it is proposed that the intensity of the sweeping signals correlates with the fast ion environment through which the hole/clump moves.

**Keywords**: Fusion plasma physics, wave-particle interaction, toroidal Alfvén eigenmode, bump-on-tail, holes and clumps.

# Publications

[A] F. Håkansson, R. M. Nyqvist and M. K. Lilley, *Directivity of Frequency Sweeping Kinetic Instabilities*, Proceedings of the 40th EPS Conference on Plasma Physics, Espoo, Finland (2013).

[B] F. Eriksson, R. M. Nyqvist and M. K. Lilley, *Kinetic Theory of Phase Space Plateaux in a Non-Thermal Energetic Particle Distribution*, Phys. Plasmas 22, 092126 (2015).

[C] F. Eriksson, R. M. Nyqvist and M. K. Lilley, *Kinetic Theory of Phase Space Plateaux*, Proceedings of the 42nd EPS Conference on Plasma Physics, Lisbon, Portugal (2015).

# Acknowledgments

I would like to express my sincerest gratitude to Dr. Robert Nyqvist for the continuous help and guidance in writing this thesis and the work presented within. I would also like to thank my co-workers, in particular my supervisor Prof. Hans Nordman for his support. Furthermore, I am grateful to Dr. Matthew Lilley and Prof. Sergei Sharapov for general guidance and the late Prof. Mietek Lisak for introducing me to the world of plasma physics. Finally, to my wonderful family, you inspire me every single day.

# Contents

# 1

# Introduction

Throughout the world there is a steadily increasing demand for energy production, more than what the current energy sources can provide for in an economically feasible and environmentally friendly manner [1]. From an environmental point of view, there are limits to how much energy can be supplied from fossil fuels such as oil and coal. Together with the increasing energy demand in the world it is clear that there is a necessity for new environmentally friendly energy sources. This is where fusion comes in.

Thermonuclear fusion is the energy source of the stars. It is the process where two nuclei merge to one nucleus that has a lower binding energy and therefore energy is released. In order to bring two positive nuclei close enough to fuse the repulsive Coulomb force needs to be overcome. The temperatures required to accomplish economically feasible thermonuclear fusion here on Earth is approximately $10^7 - 10^8$ K, which is higher than the center of the Sun. At these temperatures the gas is completely ionised and is known as a *plasma*.

The most promising candidates for fusion energy production involves the hydrogen isotopes deuterium (D) and tritium (T) in the following reactions:

$$\mathrm{D} + \mathrm{D} \longrightarrow \mathrm{He}^3 + n + 3.27 \text{ MeV} \tag{1.1a}$$

$$\mathrm{D} + \mathrm{D} \longrightarrow \mathrm{T} + \mathrm{H} + 4.05 \text{ MeV} \tag{1.1b}$$

$$\mathrm{D} + \mathrm{T} \longrightarrow \mathrm{He}^4 + n + 17.58 \text{ MeV} \tag{1.1c}$$

The reaction probability and energy output is highest for the D-T reaction, with the resulting energy shared by the neutron (80%) and the helium isotope (20%), henceforth referred to as the alpha particle, and will probably dominate future fusion experiments. However, present day experiments are mainly run with D-D reactions that have a significantly lower flux of neutrons.

In order to use nuclear fusion as an energy source the plasma needs to be confined. In stars, confinement of the plasma is provided by gravitation. Here on Earth, the current main schemes for confinement are inertial fusion and magnetic confinement. Inertial fusion is the compressing and heating of a capsule of D-T by uniform radiation from a laser. An outer layer evaporates with a resulting implosion of the capsule that creates the condition for fusion to occur. Magnetic confinement, on the other hand, uses the basic fact that a plasma consists of charged particles which follow magnetic field lines. The problem is the design of the magnetic field topology for the confinement.

Tokamaks [2] are axisymmetric, toroidal configurations that confine plasma particles through the use of an externally generated toroidal magnetic field with a smaller poloidal magnetic field generated inside the device by running currents through the plasma. There is a large number of tokamak experimental facilities operating or being constructed, the largest currently in operation is the Joint European Torus (JET), see Fig. 1.1. JET holds the world fusion power record of 16 MW from a total input power of 24 MW [3]. The largest experimental tokamak facility, currently under construction, is the internationally funded facility ITER, which will be almost twice the linear size of JET. The main objectives of ITER are to momentarily produce ten times more thermal energy from fusion heating than is supplied by auxilary heating and to maintain a substantially longer fusion pulse (up to eight to ten minutes) than current experiments [4].

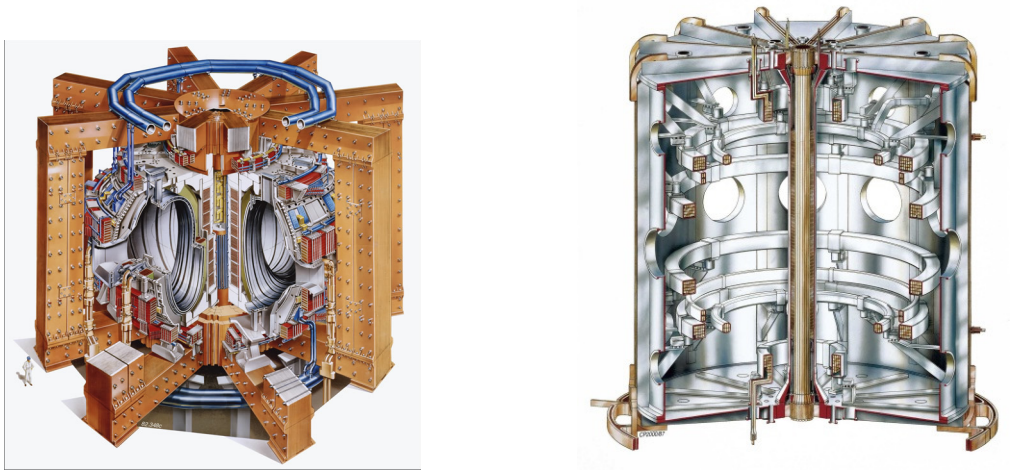

**Figure 1.1:** Graphic view of JET (left) and MAST (right), obtained from [3].

So far, the performance of a fusion facility is measured by the so called *fusion triple product*, $n_i T_i \tau_E$ [5]. Here, $n_i$ and $T_i$ are the density and temperature of ions and $\tau_E$ is the *energy confinement time*, which is the relaxation time of the plasma due to heat conduction and is tied to the plasma volume.

In tokamaks, the fusion triple product can also be expressed as $\beta\tau_E B^2$, where B is the magnetic field strength and $\beta$ is the ratio of particle to magnetic pressure. In conventional tokamaks, $\beta$ is limited to a few percent by large scale instabilities. Spherical tokamaks, like MAST (Mega Ampére Spherical Tokamak), see Fig. 1.1, are tokamaks with a large ratio of minor to major radius. This geometry allows it to operate with a considerably higher $\beta$. Note however, that the magnetic field strengh in a spherical tokamak is much lower due to restraints on the field coils by the more compact geometry.

Tokamak plasmas are heated ohmically by a current in the plasma, though external heating schemes are also necessary, such as neutral beam injection (NBI) and radio frequency heating. NBI consists of a highly energetic beam of neutrals injected into the plasma where they are ionized and heat the plasma through collisions while radio frequency waves heat the plasma through resonant interaction between circularly polarized waves and the plasma particles. In a burning fusion D-T plasma, such as in ITER, self-heating by the fusion generated alpha particles will be important to heat and maintain the plasma temperature. Common to all these heating schemes is the resulting highly energetic particles with velocities greatly exceeding the thermal velocity of ions in the plasma. As these fast particles decelerate due to collisions they transfer their energy to the background ions and electrons.

The presence of energetic ions, mainly in the plasma core, affects heating and transport of particles in the plasma [6]. These ions are not in thermodynamical equilibrium and the free energy available in their velocity distribution can destabilize wave like perturbations in the equilibrium plasma when the motion of the fast ions matches that of the wave phase velocity. A destabilization of the perturbation occurs when the fast particle pressure is large enough to overcome the total damping by the bulk plasma [7]. One important class of *magnetohydrodynamic* perturbations is the *shear Alfvén waves*. These waves oscillate at relatively low frequencies and propagate at the characteristic *Alfvén speed*. The importance of these Alfvén waves is due to the fact that the magnitude of the Alfvén speed is comparable to, or below, that of the energetic ions in the plasma. As the ions slow down they can destabilize and interact with various Alfvénic waves (cf. [8]).

The remainder of this thesis is organized as follows: In Chapter 2, we consider some properties of single charged particle motion in toroidal geometry. We also introduce the concept of waves as oscillating perturbations in electric and magnetic fields in the plasma. Focus lies on the toroidal Alfvén eigenmode (TAE), which exists due to the toroidal geometry of a tokamak. Finally, we derive an expression for the radial motion of the TAE due to its interaction with energetic particles. Chapter 3 is devoted to linear and nonlinear aspects of wave-particle interaction, where the instabilities are driven by a low density population of highly energetic particles. We will see that interaction occurs

between resonant particles travelling at roughly the phase velocity of the wave and the wave itself. This interaction leads to exponential damping/growth of the wave amplitude known as Landau damping/drive. We will employ a one-dimensional electrostatic "bump-on-tail" model to describe the nonlinear wave-particle interaction. We discuss the implications of the emergence of a phase space plateau early on in the mode evolution cycle and calculate a condition for negative wave energy and marginal stability of modes close to the plateau edges. We finish with a brief discussion on the connection between the one-dimensional model and the three dimensional tokamak geometry.

# 2

# Toroidal Systems

Magnetic confinement of plasma particles can be implemented in several different ways. Many of these methods utilize externally generated magnetic fields designed in such a way that the field lines define a torus, i.e a cylinder deformed until it closes on itself. The most common type of toroidal magnetic confinement device is the *tokamak*. In tokamaks, the plasma particles are mainly confined by means of a large magnetic field in the toroidal direction, which is generated by external coils. This results in circulating particles that follow the magnetic field lines around the torus. However, a small poloidal field component produced by a transformer induced plasma current is also necessary in order to average out radial drifts. This is because the toroidal magnetic field varies radially in space, with associated so called $\nabla B$- and curvature drifts of the particles resulting in a vertical separation of electrons and ions. The charge separation leads in turn to a potential difference and an associated $\mathbf{E}\times\mathbf{B}$- drift, which results in a radial drift outwards of both ions and electrons.

In general, a tokamak cross section may be elliptically elongated, D-shaped and asymmetric with respect to the horizontal and vertical midplanes. In this thesis, however, we will use a circular approximation described by the toroidal coordinates $(r, \theta, \zeta)$, see Fig. 2.1.

In this chapter we start by introducing the Magnetohydrodynamic model in Sec. 2.1 that is often used to analyze plasma equilibria and linear perturbations with low oscillation frequency. Then, in Sec. 2.2, we study single charged particle motion in the presence of an electromagnetic field in the toroidal geometry. We start by determining the invariants of particle motion and then use them to characterize two types of particle orbits. Finally, in Sec. 2.3, we consider Alvénic waves in cylindrical and toroidal geometry. We discuss the possible destabilization of these waves due to interaction with energetic particles and the resulting radial drift of the particles trapped in the wave field.

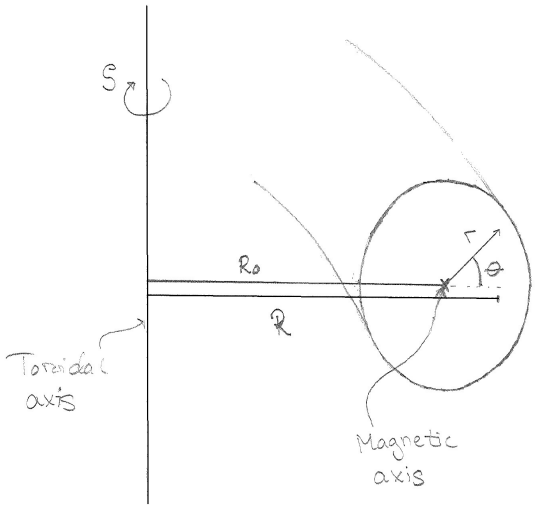


**Figure 2.1:** Poloidal cross section of a circular tokamak, displaying the toroidal coordinates $(r, \theta, \zeta)$. The distance $R_0$ from the toroidal axis to the geometric center of the cross section is called the *major radius* and the *minor radius*, $r$, denotes distances within the cross section.

## 2.1 Magnetohydrodynamic Model

MHD is a single fluid model where macroscopic properties such as densities, temperatures and pressures are used to describe the plasma. These quantities are derived from the velocity moments of the distribution function for each plasma species. When using the moment procedure, it always leads to a system of more unknowns than equations so one needs to truncate the series of moments by some proper assumptions, usually referred to as closure.

In MHD, ion and electron fluids are combined into one single fluid. For the MHD description to be valid the plasma needs to be collision dominated, i.e locally Maxwellian, which means that the MHD time scale must be sufficiently long for there to be adequately many collisions. The displacement current can then be neglected in Maxwell's equations. Without the displacement term, Ampére's law is not Lorentz invariant, which means that it is only valid for velocities much lower than the speed of light in vacuum. This is not a problem in the MHD description, since the time scale is much longer than the time it takes light to traverse the plasma. Furthermore, the dominant fluid velocity is the $\mathbf{E} \times \mathbf{B}$-drift, which means that MHD describes low frequency phenomena.

The characteristic properties of the MHD fluid are expressed by

- the total mass density

$$\rho \equiv m_i n_i + m_e n_e \ , \tag{2.1}$$

- the total charge density

$$\rho_c \equiv e(Z_i n_i - n_e) \ , \tag{2.2}$$

- the center-of-mass velocity

$$\mathbf{v} \equiv \frac{m_i n_i \mathbf{v}_i + m_e n_e \mathbf{v}_e}{m_i n_i + m_e n_e} \approx \mathbf{v}_i \ , \tag{2.3}$$

- the current density

$$\mathbf{J} \equiv e(Z_i n_i \mathbf{v}_i - n_e \mathbf{v}_e) \ , \tag{2.4}$$

- and the total scalar pressure

$$P = P_e + P_i \ , \tag{2.5}$$

where $m_i, m_e, n_i, n_e, \mathbf{v}_i$, $\mathbf{v}_e$, $P_i$ and $P_e$ are the masses, number densities, fluid velocities and pressure of ions and electrons, respectively, $Z_i$ is the ion charge number and $e$ is the magnitude of the electron charge. With the assumption of quasi-neutrality, $Z_i n_i \approx n_e$, one finds $\rho_c = 0$ and the MHD set of equations are

- the continuity equation

$$\frac{\partial \rho}{\partial t} + \nabla \cdot (\rho \mathbf{v}) = 0 \ , \tag{2.6a}$$

- the momentum equation

$$\rho \frac{d\mathbf{v}}{dt} = \mathbf{J} \times \mathbf{B} - \nabla P \ , \tag{2.6b}$$

- the adiabatic equation of state

$$\frac{d}{dt}\left(\frac{P}{\rho^\gamma}\right) = 0 \ , \tag{2.6c}$$

- the resistive Ohm's law

$$\mathbf{E} + \mathbf{v} \times \mathbf{B} = \eta \mathbf{J} \ , \tag{2.6d}$$

- Ampére's law (without the displacement current)

$$\nabla \times \mathbf{B} = \mu_0 \mathbf{J} \ , \tag{2.6e}$$

- and Faraday's law

$$\nabla \times \mathbf{E} = -\frac{\partial \mathbf{B}}{\partial t} \ . \tag{2.6f}$$

Here, $\gamma$ is the ratio of specific heats at constant pressure and constant volume, $\eta$ is the plasma resistivity and $\mu_0$ is the permeability of free space. Note that the Maxwell relation $\nabla \cdot \mathbf{B} = 0$ is implied. The fact that the displacement current is neglected in Ampére's law also means that

$$\nabla \cdot \mathbf{J} = 0 \ . \tag{2.7}$$

In many cases a further simplification is made by assuming that the plasma conductivity is high enough that the right hand side of Ohm's law can be neglected. The resulting model is called ideal MHD and one of its consequences is that the parallel component of the electric field is zero. It is not obvious that the criteria for ideal MHD are fulfilled. However, it seems to provide an accurate description of the macroscopic fusion plasma behavior [9] and is thus frequently used to describe plasma equilibrium and stability of waves. For that reason we will use it for the basic analysis of low frequency Alfvén waves in this thesis.

### 2.1.1 Equilibrium Analysis

Tokamak equilibria are efficiently analyzed by the MHD equilibrium equations (2.6) under the conditions of no time dependence ($\partial/\partial t = 0$) and no plasma flows ($\mathbf{v} = 0$). The equations describing the static plasma equilibria becomes

$$\mathbf{J} \times \mathbf{B} = \nabla P \ , \ \nabla \times \mathbf{B} = \mu_0 \mathbf{J} \ , \ \nabla \cdot \mathbf{B} = 0 \ . \tag{2.8}$$

Note that this implies that

$$\mathbf{B} \cdot \nabla P = 0 \ , \tag{2.9}$$

which means that the magnetic field lines lie on surfaces of constant pressure. Since the magnetic field has both poloidal and toroidal components, these so called flux surfaces close on themselves both toroidally and poloidally, and must therefore be nested tubes with the innermost known as the magnetic axis. Hence, $P = P(\psi)$, where $\psi$, the poloidal flux, is constant along magnetic field lines, i.e a function only of $r$. In a toroidal device the poloidal magnetic flux can be expressed as

$$\psi_P = \frac{1}{2\pi} \int_{V(r)} \mathbf{B} \cdot \nabla\theta \, \mathrm{d}^3 x \ , \tag{2.10}$$

where $\mathrm{d}^3 x = J^{-1} \mathrm{d}r\mathrm{d}\theta\mathrm{d}\zeta$, $J$ is the Jacobian and $V(r)$ is the volume bounded by the magnetic flux surface of radius $r$.

In a tokamak, we may express the magnetic field with a toroidal and a poloidal component

$$\mathbf{B} = \mathbf{B}_T + \mathbf{B}_P \ , \tag{2.11}$$

where $B_T \gg B_P$ and the toroidal magnetic field strength varies radially as $R^{-1}$:

$$B_T \equiv \frac{I(r)}{R} = \frac{B_s(r)}{1 + \epsilon \cos\theta} \ . \tag{2.12}$$

Here, $B_s \equiv I(r)/R_0$, $I(r)$ is the current in the exterior field coils, $R_0$ is the distance from the axis of symmetry to the magnetic axis and

$$\epsilon \equiv r/R_0 \ , \tag{2.13}$$

is the inverse aspect ratio, which is generally small throughout a tokamak.

### 2.1.2 Linear Stability Analysis

When we have an equilibrium plasma the next step is to look at its stability properties. To simplify the analysis we will restrict ourselves to linear stability, and represent the dependent variables as the sum of an equilibrium part plus a small perturbation,

$$\mathbf{B} = \mathbf{B}_0 + \mathbf{B}_1 \ , \quad \mathbf{J} = \mathbf{J}_0 + \mathbf{J}_1 \ , \tag{2.14a}$$

$$P = P_0 + P_1 \ , \quad \rho = \rho_0 + \rho_1 \ , \tag{2.14b}$$

where the equilibrium and perturbed quantities are denoted by the subscripts 0 and 1, respectively. We can transform the MHD equations to a frame of reference moving with the equilibrium velocity $\mathbf{v}_0$, which means that $\mathbf{v} = \mathbf{v}_1$ and, by ideal Ohm's law, $\mathbf{E} = \mathbf{E}_1$. The equilibrium quantities are then functions of space only while the perturbations are of space and time. From the set of equations (2.6a) - (2.6f), with ideal Ohm's law, we obtain sets of equations to zeroth order for the equilibrium (2.8) and to first order for the stability:

$$\frac{\partial \rho_1}{\partial t} + \nabla \cdot (\rho_0 \mathbf{v}_1) = 0 \ , \tag{2.15a}$$

$$\rho_0 \frac{\partial \mathbf{v}_1}{\partial t} = \mathbf{J}_0 \times \mathbf{B}_1 + \mathbf{J}_1 \times \mathbf{B}_0 - \nabla P_1 \ , \tag{2.15b}$$

$$\frac{\partial P_1}{\partial t} + \mathbf{v}_1 \cdot \nabla P_0 + \frac{\gamma P_0}{\rho_0} \left( \frac{\partial \rho_1}{\partial t} + \mathbf{v}_1 \cdot \nabla \rho_0 \right) = 0 \ , \tag{2.15c}$$

$$\frac{\partial \mathbf{B}_1}{\partial t} = \nabla \times (\mathbf{v}_1 \times \mathbf{B}_0) \ , \tag{2.15d}$$

$$\nabla \times \mathbf{B}_1 = \mu_0 \mathbf{J}_1 \ . \tag{2.15e}$$

Since the equilibrium equations (2.8) are independent of time, the zeroth order quantities ($\rho_0$, $P_0$, $\mathbf{B}_0$ and $\mathbf{J}_0$) take the form

$$Q_0(\mathbf{r}, t) = Q_0(\mathbf{r}) \ . \tag{2.16a}$$

The stability equations are linear, we can represent the perturbations as normal modes of frequency $\omega$

$$Q_1(\mathbf{r}, t) = Q_1(\mathbf{r}) e^{-i\omega t} \ . \tag{2.16b}$$

If we introduce the perturbed displacement vector $\vec{\xi}$ as

$$\mathbf{v}_1 = \frac{\partial \vec{\xi}}{\partial t} = -i\omega \vec{\xi}(\mathbf{r}) e^{-i\omega t} \ , \tag{2.17}$$

the linear stability equations (2.15) yield [9]

$$-\omega^2 \rho_1 \vec{\xi} = \mathbf{F}(\vec{\xi}) \ , \tag{2.18}$$

which is an eigenvalue equation with the frequency $\omega$ as the eigenvalue. Here, $\mathbf{F}$ is given by

$$\begin{aligned} \mathbf{F}(\vec{\xi}) = \frac{1}{\mu_0} \Big\{ (\nabla \times \mathbf{B}_0) \times \big[\nabla \times (\vec{\xi} \times \mathbf{B}_0)\big] + \nabla \times \Big[\nabla \times (\vec{\xi} \times \mathbf{B}_0)\Big] \times \mathbf{B}_0 \Big\} \\ + \nabla(\vec{\xi} \cdot \nabla P_0 + \gamma P_0 \nabla \cdot \vec{\xi}) \ . \end{aligned} \tag{2.19}$$

What is important to note is that $\mathbf{F}$ is Hermitian [9]. This means that $\omega^2 \in \mathfrak{R}$. If $\omega^2 > 0$ then $\omega \in \mathfrak{R}$ and the solution to (2.18) is a mode with frequency $\omega$, and if $\omega^2 < 0$ then $i\omega \equiv \gamma \in \mathfrak{R}$ and there is an instability with $Re(\omega) = 0$. The eigenvalue problem (2.18) needs to be solved for a given magnetic field in a certain geometry, with given initial values and boundary conditions. Note that, it is customary to Fourier transform.

The simplest case of a homogeneous magnetic field in an infinite geometry results in two kinds of waves, the shear and compressional Alfvén waves. For us the most interesting is the shear Alfvén wave

$$\omega^2 = k_\parallel^2 v_A^2 \ , \tag{2.20}$$

where $k_\parallel$ is the parallel wave number with respect to the magnetic field and $v_A$ is the Alfvén speed

$$v_A^2 \equiv \frac{B_0^2}{\mu_0 \rho_0} \ . \tag{2.21}$$

This wave propagates along and at angles to the magnetic background field but the fluctuation in the magnetic field is perpendicular to it (i.e $\mathbf{B}_1 \perp \mathbf{B}_0$), hence the name shear wave. Furthermore, this wave has no density or pressure fluctuations (i.e $P_1 = \rho_1 = 0$) and is therefore said to be incompressible.

## 2.2 Guiding Center Motion

In the guiding center approximation the particle motion is decomposed into a rapid gyration around the so called *guiding center position*, which drifts along the field line (with a possible acceleration/deceleration) and a drift across it. The gyrating motion is known as *Larmor gyration* and the frequency is the *cyclotron frequency*, $\omega_c$.

In the absence of wave fields, the trajectory of a particle can be characterized by the following three invariants of motion:

- the total particle energy, $E$
- the generalized toroidal momentum, $p_\zeta$
- the magnetic moment, $\mu$

To derive the invariants we use the Lagrangian for a single particle in an electromagnetic field

$$\mathcal{L} = \frac{Mv^2}{2} + Ze\left(\mathbf{v}\cdot\mathbf{A} - \phi\right) \ , \tag{2.22}$$

where $M$, $Ze$ and $\mathbf{v}$ are the mass, charge and velocity of the particle, $\phi$ and $\mathbf{A}$ are the electrostatic potential and magnetic vector potential used to describe the electric and magnetic field according to

$$\mathbf{E} = -\nabla\phi - \frac{\partial \mathbf{A}}{\partial t} \ , \tag{2.23}$$

$$\mathbf{B} = \nabla \times \mathbf{A} \ . \tag{2.24}$$

The total energy of the particle is given by $E = H$, where $H$ is the Hamiltonian of the system and can be found by the Legandre transformation [10]

$$H = \mathbf{v}\cdot\frac{\partial \mathcal{L}}{\partial \mathbf{v}} - \mathcal{L} = W + Ze\phi \ , \tag{2.25}$$

where $W$ is the particle kinetic energy. By the Euler-Lagrange equation

$$\frac{\partial \mathcal{L}}{\partial r^i} = \frac{d}{dt}\left(\frac{\partial \mathcal{L}}{\partial \dot{r}^i}\right) \ , \tag{2.26}$$

where $r^i$, $i = 1, 2, 3$, represent the coordinates (in this case $(r, \theta, \zeta)$), we find that

$$\frac{dE}{dt} = \frac{dH}{dt} = 0 \ , \tag{2.27}$$

and hence $E$ is an invariant of particle motion. Note however, that in the presence of a wave field, $\mathcal{L}$ will depend explicitly on time and $E$ is no longer invariant.

From the Lagrangian description we also find the second invariant, the generalized toroidal momentum. The individual components of the canonical momentum are given by

$$p_i = \frac{\partial \mathcal{L}}{\partial \dot{r}^i} \ . \tag{2.28}$$

By the Euler-Lagrange equation (2.26) we see that whenever the Lagrangian does not depend on a certain variable, the associated canonical momentum is an invariant. Thus, for an axisymmetric tokamak, independent on the toroidal angle $\zeta$,

$$\frac{dp_\zeta}{dt} = 0 \ , \tag{2.29}$$

where, by equations (2.22) and (2.28), the generalized momentum can be expressed as

$$p_\zeta = MR^2 \frac{d\zeta}{dt} + ZeA_\zeta \ . \tag{2.30}$$

Here, $d\zeta/dt$ is the toroidal angular velocity of the particle and $A_\zeta$ is the toroidal covariant component of the vector potential. Using the definition for the vector potential (2.24) in toroidal coordinates $(r, \theta, \zeta)$ together with the condition of axisymmetry, $\partial(..)/\partial\zeta = 0$, one obtains expressions for the radial and poloidal components of the magnetic field

$$\mathbf{B} \cdot \nabla r = J \frac{\partial A_\zeta}{\partial \theta} \ , \tag{2.31a}$$

$$\mathbf{B} \cdot \nabla \theta = -J \frac{\partial A_\zeta}{\partial r} \ . \tag{2.31b}$$

The magnetic field (2.11) has no radial component, thus, by Eq. (2.31a),

$$A_\zeta = A_\zeta(r) + C_1 \ , \tag{2.32}$$

where $C_1$ is a constant. This means that, by Eq. (2.31b),

$$A_\zeta = -\int^r \frac{\mathbf{B} \cdot \nabla \theta}{J} \, dr' + C_2 r = -\frac{1}{2\pi} \psi_P \equiv -\psi \ . \tag{2.33}$$

Here, $C_2$ is a constant, which we used Gauge freedom to set to zero, and $\psi_P$ is the poloidal flux (2.10). We can then express the toroidal momentum (2.30) as

$$p_\zeta = MR^2 \frac{d\zeta}{dt} - Ze\psi \ . \tag{2.34}$$

Note that, in the presence of an external wave field depending on $\zeta$, axisymmetry will be broken and $p_\zeta$ will no longer be invariant.

Finally, due to the periodicity of the particles gyration around a magnetic field line, it can be shown that the magnetic moment

$$\mu = \frac{Mv_L^2}{2B} \ , \tag{2.35}$$

is an adiabatic invariant, i.e constant as long as the gradients in the magnetic field are sufficiently small as compared to the plasma dimensions and the time scale of variation is long compared to the gyration frequency. This is true in a tokamak since the magnetic field varies on a large scale as compared to the radius of gyration, the *Larmor radius*, $r_L$. Here, $v_L = r_L\omega_c$ is the constant angular velocity of the gyrating particle.

As an example, when there is no electric field, $\nabla\phi = 0$, there are no accelerating forces and the particle kinetic energy

$$W = \frac{Mv^2}{2} \ , \tag{2.36}$$

is a constant of motion. Together with the magnetic moment (2.35) we then write an expression for the particle velocity parallel to the magnetic field in terms of the invariants of the particle motion,

$$v_\parallel = \pm\sqrt{\frac{2}{M}(W - \mu B)} \ , \tag{2.37}$$

which changes only due to the variation of $B$. The guiding center velocity can then be expressed as [11]

$$\mathbf{v}_{gc} = \frac{v_\parallel}{B}\mathbf{B} - \frac{v_\parallel}{B}\mathbf{B} \times \nabla\left(\frac{v_\parallel}{\omega_c}\right) \ . \tag{2.38}$$

Furthermore, when the plasma pressure is much smaller than the magnetic field pressure, $\beta \equiv P/(B^2/2\mu_0) \ll 1$, the components of the guiding center velocity, in toroidal coordinates $(r, \theta, \zeta)$, becomes

$$\frac{dr}{dt} = \hat{r} \cdot \mathbf{v}_{gc} = \frac{v_\parallel}{r}\frac{\partial}{\partial\theta}\left(\frac{v_\parallel}{\omega_c}\right) \ , \tag{2.39a}$$

$$\frac{d\theta}{dt} = \frac{\hat{\theta}}{r} \cdot \mathbf{v}_{gc} = \frac{v_\parallel}{qR_0}\left[1 - \frac{q}{\epsilon}\frac{\partial}{\partial r}\left(\frac{v_\parallel}{\omega_c}\right)\right] \ , \tag{2.39b}$$

$$\frac{d\zeta}{dt} = \frac{\hat{\zeta}}{R} \cdot \mathbf{v}_{gc} = \frac{v_\parallel}{R}\left[1 + \frac{\epsilon}{q}\frac{\partial}{\partial r}\left(\frac{v_\parallel}{\omega_c}\right)\right] \ , \tag{2.39c}$$

where $(\hat{r}, \hat{\theta}, \hat{\zeta})$ are unit vectors and $q$ is the safety factor,

$$q = \frac{\mathbf{B} \cdot \nabla\zeta}{\mathbf{B} \cdot \nabla\theta} \ , \tag{2.40}$$

i.e the number of toroidal revolutions a field line executes during one poloidal revolution.

### 2.2.1 Trapped and Passing Particles

The magnetic field in a tokamak (2.12) has a maximum poloidally. Due to the conservation of the magnetic moment $\mu$, this means that particles may bounce when approaching this maximum, depending on their ratio of perpendicular and parallel energy. Hence, there are two kinds of particles, trapped and passing particles. The trapped particles bounce toroidally and poloidally at the points where their velocities parallel to the total magnetic field vanish, while the passing particles encircle the magnetic axis and the torus toroidally and poloidally.

Following [11] we insert the expression (2.12) for the magnetic field into the expression (2.37) for the parallel velocity and obtain

$$v_\parallel = \frac{v_{\parallel 0}}{\kappa}\sqrt{\kappa^2 - \sin^2\frac{\theta}{2}}\ , \tag{2.41}$$

where we have defined the trapping parameter

$$\kappa^2 \equiv \frac{W - \mu B_s(1-\epsilon)}{2\mu B_s \epsilon}\ , \tag{2.42}$$

and

$$v_{\parallel 0} = v_\parallel(\theta = 0) = \pm\kappa\sqrt{\frac{\mu B_s \epsilon}{M}}\ . \tag{2.43}$$

Note that $W$ and $\mu$ are invariants of the particle motion, and that we have used the large aspect ratio approximation where $B_s =$ constant. Hence, $\kappa^2$ depends on the radius $r$ only through the $\epsilon$-factor. The trapped particles reverse their motion parallel to the magnetic field at the poloidal angles $\theta_B = \pm 2\arcsin\kappa$ where $v_\parallel = 0$. By conservation of energy and magnetic moment, we see that $\kappa^2 < 1$ for trapped particles, and that the passing particles satisfy $\kappa^2 > 1$. Due to the curvature and $\nabla B$-drifts, the particle orbits may also differ slightly radially from the magnetic flux surfaces. This is known as finite orbit width effects, and is the result of the second terms within the brackets on the right hand side of (2.39b) and (2.39c).

Expressions for the particle guiding center position for trapped and passing particles can in principle be calculated by integration of equations (2.39a) - (2.39c). The procedure is to transform time integrals to integrals over the poloidal angle $\theta$ using (2.39b), i.e

$$dt = \frac{qR_0}{v_\parallel}\left[1 - \frac{q}{\epsilon}\frac{\partial}{\partial r}\left(\frac{v_\parallel}{\omega_c}\right)\right]^{-1} d\theta\ . \tag{2.44}$$

In practice, however, the integrations can only be carried out as a power series in $\epsilon$. In this thesis, all integrations are performed to lowest order, which essentially means that finite orbit width effects are neglected. Thus, all quantities

in (2.44) are to be evaluated at the average particle radial position during a poloidal orbit. This means that averages over the poloidal orbits may be calculated as

$$\langle ... \rangle_B = \frac{1}{\tau_B} \int_0^{\tau_B} (...)\, \mathrm{d}t = \frac{1}{\tau_B} \int_{\theta(0)}^{\theta(\tau_B)} (...) \frac{qR_0}{v_\parallel} d\theta \ , \tag{2.45}$$

where

$$\tau_B = \int_0^{\tau_B} dt = \int_{\theta(0)}^{\theta(\tau_B)} \frac{qR_0}{v_\parallel} d\theta \ , \tag{2.46}$$

is the temporal period of a poloidal orbit, which, for passing particles, is

$$\tau_B = \int_{-\pi}^{\pi} \frac{qR_0}{v_\parallel} d\theta = \frac{4qR_0}{v_{\parallel 0}} K\left(1/\kappa\right) \ . \tag{2.47}$$

Here,

$$K(k) = \int_0^{\pi/2} \frac{1}{\sqrt{1 - k^2 \sin^2 \varphi}}\, d\varphi \ , \tag{2.48}$$

is the *complete elliptical integral of the first kind*. The poloidal frequency associated with the motion is

$$\omega_B = \frac{2\pi}{\tau_B} = \frac{\pi v_{\parallel 0}}{2qR_0 K(1/\kappa)} \ . \tag{2.49}$$

The corresponding expression for the bounce period for trapped particles between the angles $\theta_B = \pm 2 \arcsin \kappa$ becomes

$$\tau_B = \frac{8qR_0\kappa}{v_{\parallel 0}} K\left(\kappa\right) \ , \tag{2.50}$$

with the bounce frequency

$$\omega_B = \frac{2\pi}{\tau_B} = \frac{\pi v_{\parallel 0}}{4qR_0\kappa K\left(\kappa\right)} \ . \tag{2.51}$$

## 2.3 Toroidal Instabilities

We now consider a nonuniform magnetic field in a general geometry. The linearization procedure of Sec. 2.1.2 leads to the following equation [12]

$$\nabla \cdot \left( \frac{\omega^2}{v_A^2} \nabla_\perp \phi \right) + \mathbf{B}_0 \cdot \nabla \left\{ \frac{1}{B_0^2} \nabla \cdot \left[ B_0^2 \nabla_\perp \left( \frac{\mathbf{B}_0 \cdot \nabla \phi}{B_0^2} \right) \right] \right\} = 0 \ , \tag{2.52}$$

for the electrostatic potential $\phi$ of a shear Alfvén wave with high toroidal mode number and in the low $\beta$ limit, where $\nabla_\perp \phi = \mathbf{B}_0 \times (\nabla\phi \times \mathbf{B}_0)/B_0^2$.

In periodic, toroidal systems, any linear quantity may be Fourier decomposed according to

$$\phi(r,\theta,\zeta;t) = \sum_{m,n} \phi_{m,n}(r) e^{i(n\zeta - m\theta - \omega t)} \ , \tag{2.53}$$

where $m$ and $n$ are the so called poloidal and toroidal mode numbers. If the inverse aspect ratio $\epsilon$ is small, as in tokamaks, the equilibrium magnetic field is dominated by the toroidal magnetic field (2.12). This magnetic field is symmetric in $\zeta$, but because of the $\epsilon\cos\theta$ term there is no symmetry in $\theta$. For Alfvén type instabilities this leads to a coupling between neighboring poloidal harmonics of $\phi$. If we assume that the mode numbers $m$ and $n$ are large, the equations describing this coupling are [13]

$$\begin{bmatrix} \mathfrak{L}_m & \mathfrak{L}_1 \\ \mathfrak{L}_1 & \mathfrak{L}_{m-1} \end{bmatrix} \begin{bmatrix} \phi_m \\ \phi_{m-1} \end{bmatrix} = 0 \ , \tag{2.54}$$

where

$$\mathfrak{L}_m = \frac{d}{dr}\left[\left(\frac{\omega^2}{v_A^2} - k_{\parallel m}^2\right)\frac{d}{dr}\right] - \frac{m^2}{r^2}\left(\frac{\omega^2}{v_A^2} - k_{\parallel m}^2\right) \ , \tag{2.55a}$$

$$\mathfrak{L}_1 = \frac{\hat{\epsilon}}{4q^2R_0^2}\frac{d^2}{dr^2} \ . \tag{2.55b}$$

Here, the parallel wave number is given by

$$k_{\parallel m} \equiv \mathbf{k}\cdot\mathbf{B}_0/B_0 = \frac{nq(r) - m}{q(r)R_0} \ , \tag{2.56}$$

$v_A$ is the Alfvén speed (2.21) and in [14] it was shown that $\hat{\epsilon} \approx 5r/2R_0$. Note that the toroidal mode number $n$ is suppressed in Eqs. (2.54)-(2.56) since it holds for any large enough $n$.

### 2.3.1 Cylindrical Limit

In the cylindrical limit $\epsilon \to 0$, the magnetic field strength (2.12) is constant. This means that the translational symmetry in $\theta$ is restored, and the set of coupled equations (2.54) decouples into

$$\frac{d}{dr}\left[\left(\frac{\omega^2}{v_A^2} - k_{\parallel m}^2\right)\frac{d\phi_m}{dr}\right] - \frac{m^2}{r^2}\left(\frac{\omega^2}{v_A^2} - k_{\parallel m}^2\right)\phi_m = 0 \ , \tag{2.57}$$

for each poloidal harmonic. A particularly easily found branch of solutions to (2.57) has $\omega^2 = \omega_A^2 = k_{\parallel m}^2 v_A^2$. According to Eq. (2.57), however, such

modes have logaritmically divergent mode amplitudes and furthermore are almost completely damped due to the radial dispersion (well defined radial wave packages simply deconstruct since their constituents travel at different phase velocities, a process known as phase mixing) [15]. This damping is known as *continuum damping* and the radial spectrum of the logaritmically divergent modes is called *Alfvén continuum*, whose qualitative behavior is plotted in Fig. (2.2).

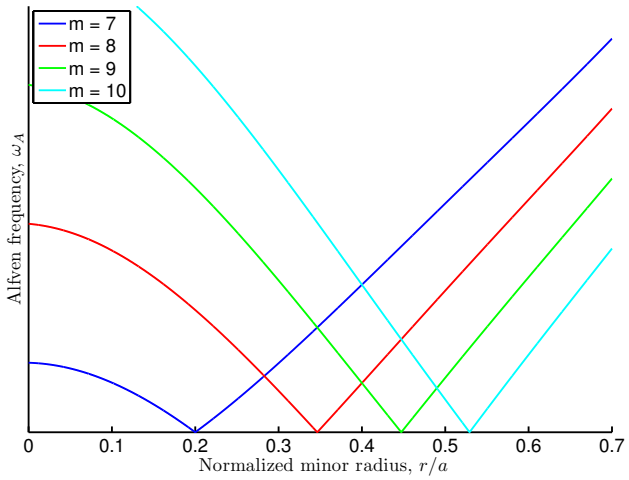


**Figure 2.2:** Qualitative figure displaying the Alfvén frequency $\omega_A$, decreasing along the branch $-k_{\parallel\, m\, n}(r)v_A(r)$ from $r = 0$ until $k_{\parallel\, m\, n} = 0$ and then increase monotonically along $k_{\parallel\, m\, n}(r)v_A(r)$ to the plasma edge, when $n = 5$ and $m$ ranges from 7 to 10.

### 2.3.2 Toroidal Alfvén Eigenmodes

Toroidal Alfvén eigenmodes (TAEs) are discrete frequency waves [16] that exist due to toroidicity induced coupling between poloidal harmonics. In the cylindrical limit, neighbouring poloidal continua cross at the surfaces $r = r_m$ (see Fig. 2.2), where

$$k_{\parallel\, m} v_A = -k_{\parallel\, m+1} v_A \equiv \omega_0 \ , \tag{2.58}$$

which implies that

$$q\left(r_m\right) \equiv q_m = \frac{2m+1}{2n} \ . \tag{2.59}$$

Inserting (2.59) in (2.58) yields

$$\omega_0 = \frac{v_A}{2q_m R_0} \ . \tag{2.60}$$

Accounting for toroidicity by letting $\epsilon$ become finite, only affects the proximity of $r_m$, where small gaps of width $\Delta\omega \approx \hat{\epsilon}\,\omega_0$ are induced in the Alfvén continuum, see Fig. 2.3. The distance between neighboring such gaps is approximately [18]

$$|r_{m+1} - r_m| \approx \frac{r_m}{nqs} \ , \tag{2.61}$$

where the magnetic shear $s$ is defined as

$$s \equiv \frac{r}{q}\frac{dq}{dr} \ . \tag{2.62}$$

Nonzero $\epsilon$ also results in a discrete frequency eigenmode, which forms due to

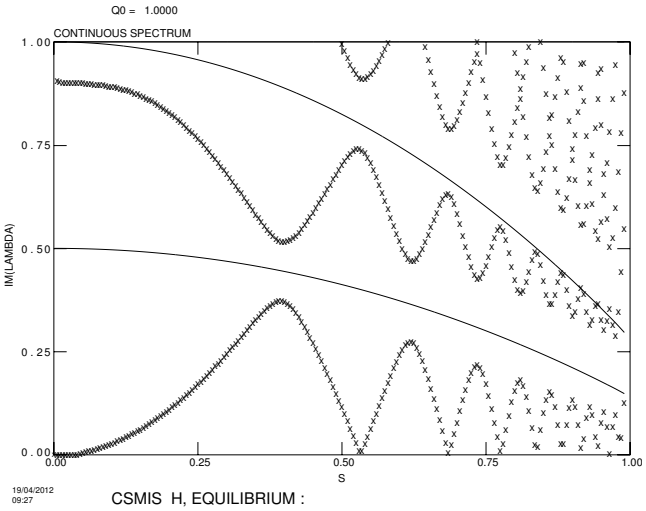


**Figure 2.3:** Alfvén continuum for $n = 4$, discharge #42979 at JET. The equilibrium was reproduced with the MHD equilibrium code HELENA [17] and the continuum by the MHD linear instability code CSCAS. Here, radial variable is $s \propto \sqrt{\psi}$ and $Im[\lambda] \propto \omega_A$.

the interaction of neighboring poloidal harmonics in the vicinity of the gap. In the low shear limit, $s \ll 1$, the distance between the gaps is sufficiently large for the eigenmode to be localized near its own gap and not interact with modes from neighboring gaps. According to boundary layer theory [18] the coupling between different harmonics takes place in a narrow inner region and in the outer region each poloidal mode satisfies the cylindrical mode equation (2.57). To determine the mode structure, a matching procedure for the outer and inner regions has to be used [18]. The result in the low shear limit is a discrete frequency eigenmode at the bottom of each toroidicity induced gap with the frequency given by

$$\omega_{TAE} = \omega_0 \left[1 - \hat{\epsilon}\left(1 - \frac{\pi^2 s^2}{8}\right)\right] \ . \tag{2.63}$$

Since the mode is inside the gap it does not fulfill the condition for continuum damping. This eigenmode is therefore weakly damped and it consists of an even combination of the coupled neighboring poloidal harmonics, see Fig. 2.4.

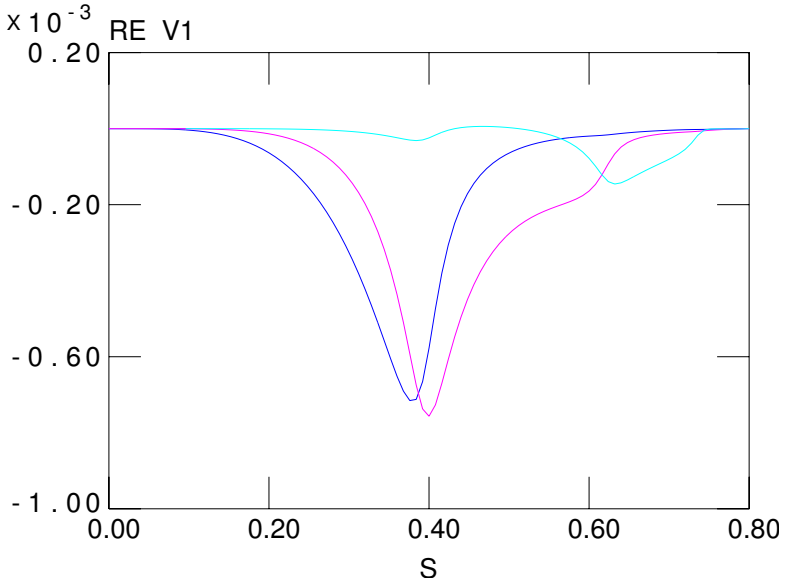


**Figure 2.4:** Radial structure for coupled, neighbouring poloidal harmonics constituting an even TAE for $n = 4$, discharge #42979 at JET with corresponding continuum in Fig. 2.3. The mode is localized around the first radial gap, but the tail of one of the poloidal harmonics reaches into the next gap. The eigenmode is found by means of the spectral MHD code MISHKA [19].

Note that to arrive at the system (2.54), ideal Ohm's law has been used, which neglects any parallel electric field. In the inner regions, we should really include both the toroidicity induced coupling and nonideal effects. The nonideal effects are due to parallel electron dynamics (from $E_{\|} \neq 0$) and first order finite ion Larmor radius (FLR) effects. Also note that the theory presented here only gives criteria for the existance of toroidal Alfvén eigenmodes. A driving mechanism is needed to excite these modes, such as e.g. resonant interaction between the wave and fast particles.

### 2.3.3 Energetic Particle Drive

The dispersion relation (2.18) has been derived within the framework of ideal MHD, using a linear approach where all quantities are assumed to consist of a stationary part and a small perturbation. This results in a real frequency $\omega = \omega_{TAE}$. Fast ions, with $v_f \gg v_{th}$, where $v_{th}$ is the thermal velocity of the bulk ions in the plasma, need to be treated using kinetic theory, which will be

presented in Sec. 3.2. The result can then be added to the MHD result, with the fast particles contributing to the imaginary part of the linear frequency, which becomes $\omega = \omega_{TAE} + i\gamma_L$ [20]. Since all perturbed quantities vary in time as $e^{-i\omega t}$, the fast particles result in an exponential growth of the wave provided that $\gamma_L > 0$. This also means that the linear theory is only valid initially.

Free energy is available to drive the mode when the fast particle pressure is large enough to overcome the total damping by the bulk plasma. For a TAE mode this is when [21, 22]

$$\frac{\gamma_L}{\omega_{TAE}} = -\left(1 - \frac{\omega_{*f}}{\omega_{TAE}}\right) F\left(\frac{v_f}{v_A}\right) \geq \frac{\gamma_d}{\omega_{TAE}} \ , \tag{2.64}$$

where $\omega_{TAE}$ is the frequency of the considered mode, $\gamma_L$ is the linear growth rate of the wave caused by the fast particles, $\omega_{*f}$ is the fast particle drift frequency and $\gamma_d$ is the total damping rate associated with the bulk plasma. The function $F\left(v_f/v_A\right)$ depends on the distribution function of the fast particles in velocity space.

In tokamaks, the fast ions gyrate in circles of radius $r_L \simeq v_f/\omega_{cf}$. Simultaneously, the density profile of the fast particles in a tokamak plasma decreases with increasing radius, which means that there are more particles that gyrate at smaller radii then at a larger radii. This produces a drift velocity in the poloidal direction called the diamagnetic drift velocity and an associated drift frequency given by [21]

$$\omega_{*f} = -\frac{m}{r}\frac{v_f^2}{\omega_{cf}}\frac{1}{p_f}\frac{dp_f}{dr} \tag{2.65}$$

where $m$ is the poloidal wave number and $\omega_{cf}$ and $p_f$ are the cyclotron frequency and the pressure of the fast ions. If $\omega_{*f}$ is larger than the wave frequency, there is an effective inversion of the velocity space distribution function gradient $\partial f/\partial v$, so that

$$\frac{\omega - \omega_{*f}}{\omega}\frac{\partial f}{\partial v} > 0 \ , \tag{2.66}$$

which means that the free energy available from the fast ions can drive the mode even when $\partial f/\partial v < 0$, cf. Chapter 3.

### 2.3.4 Paper A: Particle Motion in Frequency Sweeping Alfvénic Waves

We now consider a single isolated TAE mode in the presence of a low density population of energetic particles. After the initial exponential growth of the mode amplitude, the nonlinear TAE evolution can be analyzed using a one-dimensional "bump-on tail" model, cf. [23]. The model and its connection

to TAEs will be explained more thoroughly in Sec. 3.4. For now it suffices to mention the so called bursting type eigenmodes, the subject of Paper A, where the mode develops highly persistent sidebands with time dependent frequencies. As their frequencies evolve in time, they also move radially through the plasma. This motion can be calculated by recognizing that fast particles trapped in resonance with the wave field will follow the mode locus radially, while executing their guiding center and Larmor gyration orbits. For fast particles to be synchronized with the wave, they must satisfy a *resonance condition*

$$\omega = \langle \mathbf{k} \cdot \mathbf{v} \rangle_B \ . \tag{2.67}$$

For low frequency Alfvén waves, we will consider only the gyrocenter motion. This can be motivated by looking at the resonance condition (2.67), which, when $k_\parallel$ is given by (2.56), takes the form

$$\omega = n\omega_\zeta - m\omega_\theta + l\omega_c \ , \tag{2.68}$$

where

$$\omega_\zeta = \left\langle \frac{d\zeta}{dt} \right\rangle_B \ , \tag{2.69a}$$

$$\omega_\theta = \left\langle \frac{d\theta}{dt} \right\rangle_B \ , \tag{2.69b}$$

are the bounce averaged frequencies of toroidal and poloidal motion, $n$ and $m$ are the toroidal and poloidal mode numbers and $l \in \mathbb{N}$. Since Alfvén waves have $\omega \ll \omega_c$, we must have $l = 0$.

For simplicity, we limit ourselves to well passing particles ($\kappa^2 \gg 1$), for instance NBI generated energetic ions, in a large aspect ratio tokamak ($\epsilon \ll 1$) for which the particle drifts are negligible. The condition (2.67) for wave-particle resonance then becomes

$$\omega(t) = k_\parallel \, v_\parallel \ , \tag{2.70}$$

where $\omega(t)$ is the wave frequency, $k_\parallel$ is given by (2.56) and $v_\parallel$ is given by (2.37). We assume that $k_\parallel$ is a function of radius only through the safety factor, meaning that all equations will be evaluated at the major radius of the torus $R = R_0$. The parallel velocity (2.37) then takes the form

$$v_\parallel = \pm\sqrt{\frac{2}{m}(W - \mu B_A)} \ , \tag{2.71}$$

where $B_A = B(r = 0)$. Since $\mu$ is an adiabatic invariant, the differentiation with respect to time of equation (2.70) results in

$$\dot{\omega} = \frac{dk_\parallel}{dr} v_\parallel \dot{r} + \frac{dv_\parallel}{dW} k_\parallel \dot{W} = \frac{ms}{qR_0 r} v_\parallel \dot{r} + \frac{k_\parallel}{M v_\parallel} \dot{W} \ , \tag{2.72}$$

where $s$ is the magnetic shear, given by (2.62). The Hamiltonian of the system can be expressed as a sum of kinetic and potential energy. For particles trapped in the wave the time rate of change of the potential energy is small, so we can assume that $\dot{W} \approx \dot{H} = \dot{E}$, where $E$ is the total particle energy. We now wish to get an expression for $\dot{E}$ in terms of $r$.

In the absence of wave fields the toroidal angular momentum $p_\zeta$ is a constant of motion due to axisymmetry. In the presence of an external wave field, depending on $\zeta$ and time, the axisymmetry will be broken and $p_\zeta$ and $E$ are no longer constants of motion. However, it can be shown that, when the wave evolves slowly,

$$\dot{p_\zeta} - \frac{n}{\omega}\dot{E} = 0 \ , \tag{2.73}$$

holds. This is simply a consequence of the dependence of the perturbed wave field on $\zeta$ and $t$, which only enters as the combination $\omega t - n\zeta$ in the exponential of Eq. (2.53) when we are dealing with isolated modes with a single $n$. To lowest order in $\epsilon$, the toroidal angular momentum (2.34) can be expressed as

$$p_\zeta \approx MRv_\parallel - Ze\psi \ , \tag{2.74}$$

where we have used (2.39c). Furthermore, in this limit, the poloidal magnetic flux (2.10) becomes

$$\psi \approx B_A \int_0^r \frac{r'}{q(r')}\,\mathrm{d}r' \ . \tag{2.75}$$

Note that all quantities denoted with the subscript 0 are to be evaluated at the magnetic axis and those not labeled with 0 are taken at the bounce averaged radius. After bounce averaging and differentiation with respect to time

$$\dot{\psi} = \frac{1}{Ze}\left(M\frac{d}{dt}\left\langle Rv_\parallel\right\rangle_B - \dot{p_\zeta}\right) \ . \tag{2.76}$$

By Eq. (2.45), for well passing particles with $\theta(0) = -\pi$ and $\theta(\tau_B) = \pi$, we get

$$\left\langle Rv_\parallel\right\rangle_B \approx 2\pi\frac{qR_0^2}{\tau_B} \approx R_0 v_{\parallel 0} \ , \tag{2.77}$$

where the bounce time (2.47) has been used in the limit of well passing particles. Inserting (2.73) and (2.77) into (2.76) yields the expression for $\dot{E}$, which substituted into (2.72) gives the radial drift of the particles as

$$\frac{\dot{r}}{r} = -\frac{\dot{\omega}}{\omega_c}\frac{m}{k_\parallel^2 r^2}\left(1 - \frac{m^2 s}{k_\parallel^3 r^2 qR}\frac{\omega}{\omega_c}\right)^{-1} \ . \tag{2.78}$$

A similar expression can be calculated for deeply trapped particles ($\kappa^2 \ll 1$) using the resonance condition (2.68). The bounce averaged frequency of poloidal

motion is given by Eq. (2.51) in the limit of deeply trapped particles and the bounce averaged frequency of toroidal motion is calculated using (2.69a). The resulting radial drift can be expressed as

$$\frac{\dot{r}}{r} = -\dot{\omega}\left((1-s)\omega + m\left(\frac{3}{2} - 2s\right)\omega_\theta\right)^{-1} \quad . \tag{2.79}$$

# 3

# Nonlinear Wave-Particle Interaction

We now proceed to study the nonlinear evolution of fast particle driven modes. This is important in order to establish the long term effect of the fast particles on the overall plasma confinement and performance. E.g., it has been demonstrated that well established, saturated TAEs with benign mode amplitudes are capable of transporting and redistributing fast particles, which might have a detrimental effect on the plasma confinement as a whole [24]. Also, even though more ferociously evolving TAEs have traditionally been associated with local (phase space) perturbations, it has lately been suggested that such behavior may entirely deplete he plasma of fast particles [25]. In this thesis we limit ourselves to the study of single, isolates modes, which is motivated when the modes are well separated in phase space so that their regions of influence do not significantly overlap. By means of action-angle variables and the framework of canonical transformations, particle motion in a single TAE mode with reasonably well defined frequency can be described by a one dimensional model where the equations look very much like fluid equations [26]. For TAEs, this can be conceptually understood since even in the presence of a TAE field the particle motion is characterized by two constants of motion. The first is the magnetic moment $\mu$, which remains constant due to the fact that the TAE frequency is much smaller than the ion cyclotron frequency. The second is a combination of the toroidal canonical momenta $p_\zeta$ and the total particle energy $E$, see Eq. (2.73).

In this chapter we start by considering electrostatic longitudinal waves in a one dimensional uniform plasma. In Sec. 3.1 the plasma is considered cold and a fluid description is used to describe the mode oscillations. Then, in Sec. 3.2, thermal effects are included, which leads to a dispersive dependence

of the mode frequency on the wave number. *Kinetic theory* is then employed to further investigate the effect of finite plasma particle velocities, and we will see that this leads to substantial interaction between a group of particles travelling at roughly the *phase velocity* of the wave and the wave itself. Those particles are called resonant, and their interaction with the wave leads to exponential damping (or growth) of the wave amplitude, known as Landau damping/drive, that is phenomenonically described in Sec. 3.3. In Sec. 3.4 we consider the evolution of fast particle driven instabilities using a simple one dimensional electrostatic "bump-on-tail" model, in which the resonance lies in the high energy tail of the distribution from the bulk plasma and a bunch of extra particles have been added around the resonance to mimic fast particles in a tokamak. Within the bump-on-tail description, inclusion of dissipation in the main plasma, modeled in the simplest possible fashion via a friction force term in the background plasma fluid equations, reveils the emergence of a *phase space plateau* during the nonlinear phase. It is our belief that the structure and dynamics of this plateau, with modes close to its edges referred to as *edge modes* in Papers B and C, directly determines the nonlinear mode evolution life cycle. In Sec. 3.5 we derive a condition for negative energy for these edge modes. Then, in Sec. 3.6, we study the case of marginal stability of the edge modes with a smooth plateau distribution. Finally, in Sec. 3.7, we make a connection between the one dimensional model and the three dimensional geometry of a tokamak.

## 3.1 Electrostatic Plasma Waves in a Cold Plasma

We consider an electrostatic wave with spatial period $\lambda$ and wave number $k = 2\pi/\lambda$ in a one-dimensional uniform, static plasma fulfilling $v_{th} \ll \omega/k$, where $v_{th}$ is the thermal velocity of the electrons and $\omega$ is the wave carrier frequency. The wave can be treated as a small perturbation to the stationary and homogeneous background plasma, which in this limit is considered cold. The wave frequency is high enough that the ions are unaffected by the wave field due to their much larger mass, and therefore do not contribute to the dynamics except to keep the equilibrium plasma neutral, $n_i = n_{i0}$. The electron density and velocity on the other hand are decomposed as an unperturbed part and a small perturbation, $n_e = n_{e0} + \delta n_e$ and $v_e = v_{e0} + \delta v_e$, where $n_{e0} = n_{i0}$ and we set $v_{e0} = 0$. As always in connection with the latter assumption, we consider the case when the electric field, $E(x;t)$, is purely a wave quantity and thus has no equilibrium part either, so that there is no net acceleration of the plasma as a whole. We assume that the electric field is small enough that fluid nonlinearities are unimportant. The electrons then respond linearly to the electric field and their perturbed velocity and perturbed density satisfies

the linearized fluid equation of motion and the continuity equation

$$\frac{\partial \delta v_e}{\partial t} = -\frac{e}{m_e} E \ , \tag{3.1a}$$

$$\frac{\partial \delta n_e}{\partial t} + n_{e0} \frac{\partial \delta v_e}{\partial x} = 0 \ , \tag{3.1b}$$

where $e$ and $m_e$ are the (magnitude of the) charge and mass of the electron, respectively. Now, the Poisson equation provides closure,

$$\frac{\partial E}{\partial x} = \frac{e}{\epsilon_0}(n_i - n_e) = -\frac{e}{\epsilon_0}\delta n_e \ , \tag{3.2}$$

where $\epsilon_0$ is the permittivity of free space. We express the electric field using the electrostatic potential $E = -\partial\Phi/\partial x$, and since the equations are linear we Fourier expand the perturbed quantities,

$$\Phi, \delta v_e, \delta n_e \sim e^{i(kx-\omega t)} \ . \tag{3.3}$$

The differential equations (3.1) - (3.2) then become algebraic and can be combined to give the *dispersion relation*

$$\omega^2 = \omega_{pe}^2 \equiv \frac{e^2 n_{e0}}{\epsilon_0 m_e} \ . \tag{3.4}$$

i.e a function on the form $\omega = \omega(k)$. This wave is called the longitudinal wave since it propagates parallel to the electric field. The lack of an oscillating magnetic field makes this a purely electrostatic wave. Also, there is no depencence on $k$ in the dispersion relation, which means that there is no dispersive effect. This is the reason that we will later choose this particular mode to emulate a TAE mode in Section 3.4.

## 3.2 Warm Plasma Waves: Linear Landau Damping

The effect of thermal plasma particle motion on the system described in the previous section is obtained by the inclusion of a nonzero electron pressure term in (3.1a) and an equation of state relating the electron pressure and density. The dispersion relation (3.4) gets a small thermal correction and becomes (cf. [27])

$$\omega^2 = \omega_{pe}^2 + \frac{3k_B T}{m_e} k^2 \ , \tag{3.5}$$

where $k_B$ is Bolzmanns constant and $T$ is the temperature of the electron fluid. This thermal correction introduces dispersion of the wave by the inclusion of

a $k$-dependent term, but the method misses the important hot-plasma contribution from particles energetic enough to interact resonantly with the wave field. In order to describe wave-particle interaction kinetic theory is used. The plasma is described in terms of a *distribution function* $f(x, v, t)$, where $f(x, v, t)dxdv$ is the probability of finding particles within the *phase space* element of volume $dxdv$, centered at $(x, v)$. The distribution function $f$ evolves in phase space according to the *Vlasov equation*

$$\frac{\partial f}{\partial t} + \dot{x}\frac{\partial f}{\partial x} + \dot{v}\frac{\partial f}{\partial v} = 0 \ , \tag{3.6}$$

where $\dot{v} = -eE/m_e$ and particle-particle interactions (collisions) have been neglected. We consider a perturbative solution by expansion of the distribution function according to

$$f = F_0 + \delta f \ . \tag{3.7}$$

Here, $F_0$ is the equilibrium, or *unperturbed*, distribution function in the absence of wave fields. It is static by definition, $\partial F_0/\partial t = 0$. Also, the uniform equilibrium plasma fulfills $\partial F_0/\partial x = 0$ which means that $F_0 = F_0(v)$. The term $\delta f \ll F_0$, is a perturbation from the equilibrium distribution due to the wave field. To linear order, the Vlasov equation (3.6) becomes,

$$\frac{\partial \delta f}{\partial t} + v\frac{\partial \delta f}{\partial x} - \frac{eE}{m_e}\frac{dF_0}{dv} = 0 \ . \tag{3.8}$$

We Fourier expand the perturbed quantities,

$$E, \delta f \sim e^{i(kx-\omega t)} \ , \tag{3.9}$$

and Eq. (3.8) becomes an algebraic expression for the perturbed distribution function

$$\delta f = i\frac{eE}{m_e}\frac{dF_0/dv}{\omega - kv} \ . \tag{3.10}$$

The Poisson equation once again provides closure,

$$\frac{\partial E}{\partial x} = -\frac{e}{\epsilon_0}\delta n_e = -\frac{e}{\epsilon_0}\int \delta f \, dv \ , \tag{3.11}$$

which by Fourier expansion, together with (3.10) result in a dispersion relation on the form,

$$1 + \frac{\omega_{pe}^2}{k}\int \frac{d\hat{F}_0/dv}{\omega - kv}\, dv = 0 \ . \tag{3.12}$$

Here, $\hat{F}_0$ is normalized with $n_{e0}$ so that $\int \hat{F}_0(v)\, dv = 1$. Note that the integral in Eq. (3.12) diverges at $v = \omega/k$. This means that the particles with velocities close to this *resonant velocity* will interact heavily with the wave. Landau was

the first to properly treat this integral [28]. For the weakly damped high frequency wave ($v_{th} << \omega/k$) we calculate an approximate solution when $\hat{F}_0$ is taken to be a Maxwellian distribution function,

$$\hat{F}_0 = \frac{1}{\sqrt{\pi} v_{th}} e^{-v^2/v_{th}^2} \ , \tag{3.13}$$

where the thermal velocity $v_{th}$ is defined using

$$\frac{m_e v_{th}^2}{2} \equiv k_B T \ . \tag{3.14}$$

In the weakly damped case Im[$\omega$] is small and the integration contour is a straight line along the Re[$v$] axis with a small semicircle *under the pole* at $v = \omega/k$. Eq. (3.12) becomes (cf. [29])

$$1 - \frac{\omega_{pe}^2}{k^2} \left[ P \int_{-\infty}^{\infty} \frac{d\hat{F}_0/dv}{v - \omega/k} \, dv + i\pi \left. \frac{d\hat{F}_0}{dv} \right|_{v=\frac{\omega}{k}} \right] = 0 \ , \tag{3.15}$$

where the first term inside the bracket is the *Cauchy principal value* of the integral and the second is $i\pi$ times the *residue* at the pole, corresponding to the contribution from the nonresonant particles and the resonant particles, respectively. For the nonresonant particles, $d\hat{F}_0/dv$ is negligably small for large enough velocities, say $nv_{th}$ ($n > 1$), which allows us to limit the evaluation of the integral to this velocity. In this limit we Taylor expand,

$$\frac{1}{v - \omega/k} \simeq -\frac{k}{\omega} \left[ 1 - \frac{kv}{\omega} - \left( \frac{kv}{\omega} \right)^2 - \left( \frac{kv}{\omega} \right)^3 \right] \ . \tag{3.16}$$

and the integral in (3.15) now consist of four terms

$$P \int_{-\infty}^{\infty} \frac{d\hat{F}_0/dv}{v - \omega/k} \, dv \approx \frac{2}{\sqrt{\pi} v_{th}^3} \int_{-\infty}^{nv_{th}} \frac{kv}{\omega} \left[ 1 - \frac{kv}{\omega} - \left( \frac{kv}{\omega} \right)^2 - \left( \frac{kv}{\omega} \right)^3 \right] e^{-v^2/v_{th}^2} \, dv \ , \tag{3.17}$$

Now, we expand the integration limit to infinity once again, since any errors this might bring in the Taylor expansion are suppressed by the exponential. In this high frequency limit the first and third terms goes to zero and by calculation of the integral from the second and fourth term we obtain an expression for (3.15) on the form

$$D(\omega) = 1 - \frac{\omega_{pe}^2}{\omega^2} - \frac{3k^2 v_{th}^2}{2} \frac{\omega_{pe}^2}{\omega^4} - i\pi \frac{\omega_{pe}^2}{k^2} \left. \frac{d\hat{F}_0}{dv} \right|_{v=\frac{\omega}{k}} = 0 \ . \tag{3.18}$$

We proceed to find a solution by setting

$$\omega = \omega_R + i\omega_I \ , \tag{3.19}$$

thus,

$$D(\omega) = D_R(\omega_R + i\omega_I) + iD_I(\omega_R + i\omega_I) = 0 \ , \tag{3.20}$$

which we Taylor expand around $\omega_R$ assuming a weak damping, i.e. $\omega_I \ll \omega_R$,

$$D_R(\omega_R)+(\omega-\omega_R)\left.\frac{dD_R}{d\omega}\right|_{\omega=\omega_R}+i\left[D_I(\omega_R)+(\omega-\omega_R)\left.\frac{dD_I}{d\omega}\right|_{\omega=\omega_R}\right]=0\ . \tag{3.21}$$

The real and imaginary parts need to be zero separately

$$D_R(\omega_R) - \omega_I \left.\frac{dD_I}{d\omega}\right|_{\omega=\omega_R} = 0 \ , \tag{3.22a}$$

$$D_I(\omega_R) + \omega_I \left.\frac{dD_R}{d\omega}\right|_{\omega=\omega_R} = 0 \ . \tag{3.22b}$$

In (3.22a) the second term is much smaller and therefore neglected, thus,

$$D_R(\omega_R) \simeq 0 \ , \tag{3.23a}$$

$$\omega_I = -\frac{D_I(\omega_R)}{\left.\frac{dD_R}{d\omega}\right|_{\omega=\omega_R}} \ . \tag{3.23b}$$

We set

$$\omega_R^2 = \omega_{pe}^2(1+\delta) \ , \tag{3.24}$$

where $0 \leq \delta \ll 1$. Eq. (3.23a) becomes,

$$\omega_{pe}^2(1+\delta) = \omega_{pe}^2\left[1+\frac{3k^2v_{th}^2}{2\omega_{pe}^2(1+\delta)}\right] \approx \omega_{pe}^2\left[1+\frac{3k^2v_{th}^2(1-\delta)}{2\omega_{pe}^2}\right] \ . \tag{3.25}$$

Here, $v_{th}^2 \ll \omega_{pe}^2/k^2$ so to lowest order $\delta = 3k^2v_{th}^2/2\omega_{pe}^2$ and

$$\omega_R^2 = \omega_{pe}^2 + \frac{3v_{th}^2}{2}k^2 \ , \tag{3.26}$$

which is the same result we got using fluid theory (3.5). By an analogous calculation Eq. (3.23b) can, to lowest order, be expressed as

$$\omega_I = \frac{\pi\omega_{pe}^3}{2k^2}\left.\frac{d\hat{F}_0}{dv}\right|_{v=\frac{\omega_R}{k}} \ . \tag{3.27}$$

Note that $\omega_I$ indeed is small as compared to $\omega_R$, and so we may express the dispersion relation as

$$\omega = \omega_{pe} + \frac{3v_{th}^2}{4}k^2 + i\gamma_L \ , \tag{3.28}$$

where

$$\gamma_L \equiv \frac{\pi\omega_{pe}^3}{2n_{e0}k^2} \left.\frac{dF_0}{dv}\right|_{v=\frac{\omega}{k}} \ . \tag{3.29}$$

Since the equilibrium distribution function $F_0$ is taken as a Maxwellian the slope of the distribution function at the *phase velocity* of the wave $v_{ph} = \omega/k$ is negative which result in a negative $\gamma_L$ and the wave amplitude experiences damping from the interaction with the resonant particles. This phenomenon is called *Landau damping* and it is not found within the fluid description of the plasma.

## 3.3 Nonlinear Landau Damping

An intuitive understanding of Landau damping can be gained by studying the motion of single particles in a given electric field

$$E = A\cos(kx - \omega_{pe}t) \ . \tag{3.30}$$

We make a change of variables to a frame that moves at the wave phase velocity

$$kz = kx - \omega_{pe}t - \frac{\pi}{2} \ , \tag{3.31}$$

and the total energy of a particle in this frame of reference is

$$W = \frac{m_e}{2}u^2 + \frac{eA}{k}\cos(kz) \ , \tag{3.32}$$

where

$$u \equiv v - \frac{\omega_{pe}}{k} \tag{3.33}$$

is the wave-frame velocity. Note that $W$ is essentially the wave frame Hamiltonian, and is therefore a conserved quantity of the particle motion when the electric field amplitude $A$ does not change. We set

$$\omega_A \equiv \sqrt{\frac{eAk}{m_e}} \ , \tag{3.34}$$

which corresponds to a normalization of the mode amplitude that has the dimension of frequency, and invert Eq. (3.32) to give an expression for the particle velocity as function of $z$, given a value of $W$,

$$u(z;W) = \pm\sqrt{2\left(\frac{W}{m_e} - \frac{\omega_A^2}{k^2}\cos(kz)\right)} \ . \tag{3.35}$$

In Fig. 3.1 the trajectories of energy $W$ are visualized in phase space. The gray trajectories with $u > 0$ are called co-passing and describe flows in the direction of increasing $z$, while those with $u < 0$ are called counter-passing and describe flows in the direction of decreasing $z$. The particles inside the so called *separatrix* (the red curve) are called trapped. The trapped particles bounce back and forth with a bounce period given by

$$\tau_B = \int_{z_2}^{z_2} \frac{dz}{u} = \int_{z_1}^{z_2} \left[ 2 \left( \frac{W}{m_e} - \frac{\omega_A^2}{k^2} \cos(kz) \right) \right]^{-1/2} dz \ , \tag{3.36}$$

where $z_1$ and $z_2$ are the turning points at which the total energy of the particle matches the electrostatic potential energy, i.e. $u(z_{1,2}; W) = 0$. By performing the integration in (3.36) we get

$$\tau_B = \frac{4}{\omega_A} K(\kappa) \ . \tag{3.37}$$

Here, $K(\kappa)$ is the complete elliptical integral of the first kind as given by (2.48) and we have defined

$$\kappa^2 \equiv \frac{1}{2} \left( \frac{kW}{eA} + 1 \right) < 1 \ . \tag{3.38}$$

The bounce frequency for the trapped particles is then given by

$$\omega_B(W) = \frac{2\pi}{\tau_B} = \frac{\pi \omega_A}{2K(\kappa(W))} \ , \tag{3.39}$$

as illustrated in Fig. 3.2 for different values of $\omega_A$.

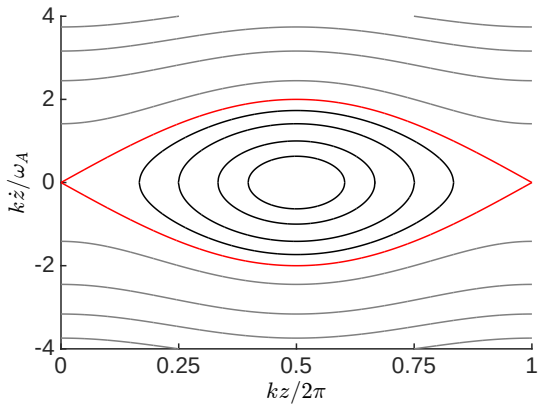


**Figure 3.1:** *Phase space trajectories of particles in the presence of a sinusoidal electric field* (3.30)*. The wave frame velocity* (3.35) *is normalized in units of* $\omega_A/k$ *as defined in Eq.* (3.34)*. The separatrix is highlighted in red.*

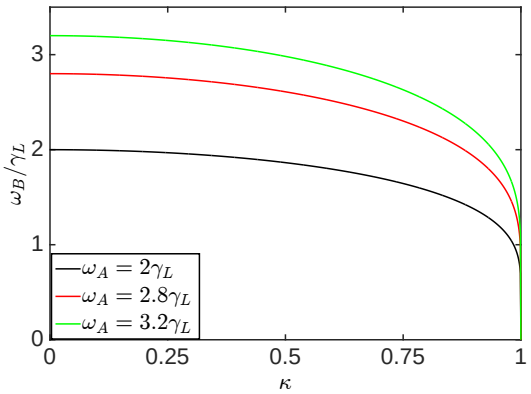


**Figure 3.2:** *Bounce frequency of trapped particles for different values of $\omega_A$. Here $\kappa = 0$ corresponds to the most deeply trapped particle orbit and $\kappa = 1$ corresponds to the separatrix orbit.*

The energy dependence of $\omega_B$ is the basic mechanism behind Landau damping. As shown in Fig. 3.2, it means that trapped particles on different orbits complete their periodic motion at different rates. Particles on deeply trapped trajectories have $\omega_B \sim \omega_A$, but the ones further out revolve at lower rates that tends to 0 at the separatrix orbit. Over time, this variation leads to a phenomenon called *phase mixing* (cf. continuum damping for Alfvén eigenmodes in Sec. 2.3): The skewed orbital frequency profiles effectively averages the particle distribution along the trajectories until it becomes entirely flat throughout the eye-shaped trapped particle area (the region of phase space inside the separatrix). Furthermore, redistribution of particles changes their kinetic energy, so in order for the total energy to remain constant there must be a corresponding energy exchange between the particles and the wave, which means that the wave amplitude $\omega_A$ must evolve as a result of the flattening. Consider the case when $dF_0/dv < 0$ at the resonant velocity $v = \omega_{pe}/k$ at $t = 0$, as it is e.g. for the Maxwellian considered in the previous section. Initially, there are more trapped particles in the lower half of the phase space plot in Fig. 3.1 i.e. with velocities just below the phase velocity. So as the phase mixing flattens out the distribution inside the separatrix there is a net transport of particles to higher velocities. That is, a flux of energy from the wave to the particles, which results in a decrease of the wave amplitude referred to as nonlinear Landau damping. Linear Landau damping is recovered within this picture if the perturbation of the distribution function is small enough that the linearized model equation (3.8) remains valid, i.e if the wave is extinguished before the particles complete a full orbit.

Nonlinear effects also dominates if the flux of energy is from the particles to the wave (i.e when $dF_0/dv > 0$ at $v = \omega_{pe}/k$ at $t = 0$) resulting in a drive

instead of a damping. Nonlinear analysis in the case of Landau drive will be the subject of Sec. 3.4, however, for now it suffices to say that the mode amplitude will saturate due to phase mixing and, in principle, an energy balance analysis can be carried out to determine a saturation level of the mode amplitude.

## 3.4 Bump-on-Tail Model

A low density population of highly energetic electrons is now added to the main or *bulk* plasma. The result is a small "bump" on the tail of the distribution function for the bulk plasma, cf. Fig. 3.3. We are still considering a one dimensional electrostatic plasma wave with a prescribed wavelength $\lambda$ and wave number $k = 2\pi/\lambda$ in a uniform plasma equilibrium. The wave carrier frequency is assumed to be high enough that the plasma can be separated as a cold bulk whose response can be described using fluid theory while the energetic electrons, which may interact resonantly with the wave, must be treated separately. We include a linear friction force with a damping rate $\gamma_d$, used to mock up dissipative wave damping in the real plasma [30–33], thereby damping the velocity perturbations and the linear fluid equation (3.1a) now takes the form

$$\frac{\partial \delta v_e}{\partial t} = -\frac{e}{m_e} E - 2\gamma_d \delta v_e \ . \tag{3.40}$$

The damping rate $\gamma_d$ is assumed to be significantly smaller than the wave carrier frequency, which in turn is assumed to remain close to the electron plasma frequency $\omega_{pe}$ in order to accurately represent the electric field as a single, possibly modulated, sinusoidal mode that oscillates at $\omega_{pe}$,

$$E(x,t) = A(t)\cos(kx - \omega_{pe} t) \ , \tag{3.41}$$

where the amplitude $A(t)$ is assumed to evolve slowly in time as compared with the mode oscillations, $d \ln A/dt \ll \omega_{pe}$.

The energetic electrons are described kinetically in terms of their phase space distribution function $f(x, v, t)$. Just as in the previous section $f$ is decomposed according to Eq. (3.7). Note however that $f$ is now only for the energetic electrons and not the bulk electrons. This means that the Poisson equation (3.2) has an extra term from the energetic electrons and becomes

$$\frac{\partial E}{\partial x} = -\frac{e}{\epsilon_0}\left[\delta n_e + \int \delta f dv\right] \ . \tag{3.42}$$

The kinetic equation (3.8) governing the evolution of the distribution function $f$ is taken as

$$\frac{\partial f}{\partial t} + v\frac{\partial f}{\partial x} - \frac{e}{m} E \frac{\partial f}{\partial v} = \mathfrak{C}\big[f\big] + S\,(v) \ . \tag{3.43}$$

The right hand side represents fast particle collisions and sources, whose combined action is to relax $f$ towards an equilibrium distribution $F_0(v)$ that, for simplicity, is taken as a constant, positive slope throughout the wave-particle resonance. It is modeled as the following combination of three operators (cf. [34])

$$\mathfrak{C}[f] + S(v) = -\beta\big(f - F_0\big) + \frac{\alpha^2}{k}\frac{\partial}{\partial v}\big(f - F_0\big) + \frac{\nu^3}{k^2}\frac{\partial^2}{\partial v^2}\big(f - F_0\big)\,. \qquad (3.44)$$

The first term is essentially a sink that relaxes the distribution function $f$ to the equilibrium distribution at rate $\beta$. It is called the Krook operator, and is often used to mock up the effect of more challenging operators. The second term represents the effect of slowing down of the energetic electrons due to collisions with the cold particles, and is denoted collisional drag. Note that the drag operator consists of two parts. The first part acts as a contant force that slows the particles down and the second acts as a sink that preserves the equilibrium distribution function $F_0$. Finally, the third term in Eq. (3.44) is a velocity space diffusion operator with constant diffusion coefficient. It is included in order to represent energy space diffusion of energetic plasma particles, which is actually the dominant collisional process at low particle energy, but also to mimic the effect of stochastic scattering in localized but overlapping resonances, such as e.g. during RF heating.

All simulations in the remainder of this chapter are computed using a fully nonlinear algoritm, previously described in Ref. [35] and currently available online [36], that, given a profile for $F_0$ and values for $\gamma_d$, $\beta$, $\alpha$ and $\nu$, solves Eqs. (3.40), (3.42) and (3.43) for the nonlinear evolution of $E(x,t)$ and $f(x,v,t)$.

### 3.4.1 Saturation of Mode Amplitude in the Non-Dissipative Bump-on-Tail Instability

We consider the collisionless, dissipationless bump-on-tail instability ($\beta = \alpha = \nu = \gamma_d = 0$). The fast particle equilibrium distribution $F_0$ causes the electric field amplitude, depicted in Fig. 3.4, to grow at a linear rate $\gamma_L \propto dF_0/dv$ due to energy released by phase mixing. The velocity width of the separatrix in Fig. 3.1 is proportional to $\sqrt{A}$ which means that as the amplitude grows the velocity width increases and passing particles on orbits just outside the separatrix become trapped. Eventually no more energy can be extracted by phase mixing and the amplitude saturates at $\omega_A = 3.2\gamma_L$ [37]. However, as shown in Fig. 3.4, the saturation level is modulated, which is due to the presence of narrow circulating bands of particles on barely trapped orbits just inside the separatrix, as can be seen in Fig. 3.5.

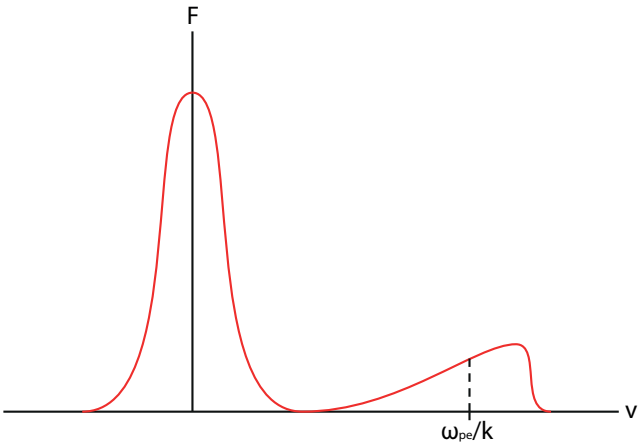


**Figure 3.3:** *Cartoon illustrating the bump-on-tail distribution function. The contribution from the cold electrons is treated using fluid theory and the contribution from the energetic particles is taken as a constant positive slope throughout the wave-particle resonance.*

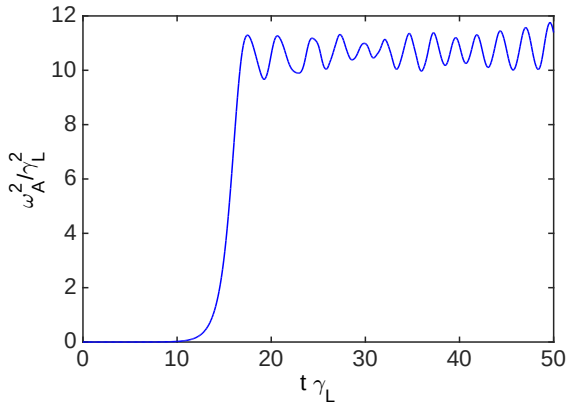


**Figure 3.4:** *Mode amplitude evolution of a plasma eigenmode excited by the presence of energetic particles in the collisionless, dissipationelss limit.*

The saturated mode amplitude can be calculated by balancing the energy lost from the energetic electrons to that gained by the wave. The initial state is taken as the equilibrium distribution consisting of a constant positive slope throughout the wave-particle resonance and the final saturated state is taken as the fully phase mixed equilibrium distribution. In Fig. 3.1 we observe that the particle trajectories most affected by interaction with the wave field are the trapped particle trajectories. As a first approximation we therefore neglect the contribution from the passing particles and only consider the orbits inside the separatrix where the distribution is completely flat and takes on the value of the equilibrium distribution function at the resonance. The energy difference between the initial equilibrium and the final saturated state (per wavelength

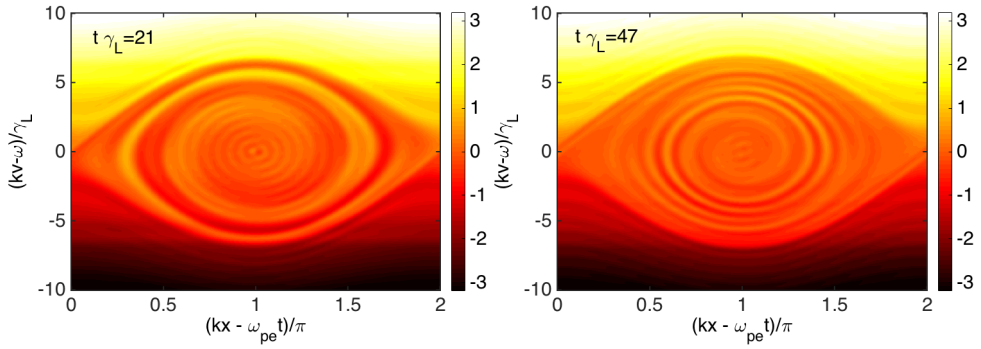


**Figure 3.5:** *Phase space plot illustrating phase mixing of trapped particles in the collisionless, dissipationless limit at two different times. Initially, there are narrow circulating bands of particles, remnants of imperfect phase mixing, on barely trapped orbits (left) which are gradually reduced (right).*

$\lambda$) is

$$\Delta E = E_0 - E_{sat} = \frac{m_e}{2} \int_0^{\lambda} \int_{-\infty}^{\infty} v^2 (F_0 - F_{sat})\, dv\, dx \ . \tag{3.45}$$

Using the wave frame coordinates defined in (3.31), and (3.33) the initial and final distributions are

$$F_0 = C + \left. \frac{dF_0}{du} \right|_{u=0} u \ , \tag{3.46}$$

and

$$F_{sat} = C \ , \tag{3.47}$$

so Eq. (3.45) becomes

$$\Delta E = \frac{2 m_e \omega_{pe}}{k} \left. \frac{dF_0}{du} \right|_{u=0} \int_0^{\lambda} \int_0^{u_s(z)} u^2 \, du \, dz \ , \tag{3.48}$$

where $u_s = u_s(z)$ is the wave frame velocity at the separatrix. Using Eq. (3.35) for the particle velocity and $\lambda = 2\pi/k$, we calculate the energy difference to be

$$\Delta E = \frac{2^7}{3^2} \frac{m_e \omega_{pe} \omega_A^3}{k^5} \left. \frac{dF_0}{du} \right|_{u=0} \ . \tag{3.49}$$

Note that $\Delta E$ is positive, which means that the particles have lost energy to the wave, as expected. We balance this energy with the kinetic and electrostatic energy associated with the perturbed quantities $\delta v_e$ and $E$. Given a sinusoidal electric field (3.30), the linearized fluid equation of motion (3.1) allows us to express the kinetic energy density as

$$K = \frac{n_{e0} m_e \delta v_e^2}{2} = \frac{n_{e0} e^2 A^2}{2 m_e \omega_{pe}^2} \sin^2(kx - \omega_{pe} t) = \frac{\epsilon_0 A^2}{2} \cos^2(kz) \ , \tag{3.50}$$

and the electrostatic energy density is

$$U = \frac{\epsilon_0 E^2}{2} = \frac{\epsilon_0 A^2}{2} \sin^2(kz) \ . \tag{3.51}$$

Thus, the total energy (per wavelength) is

$$\int_0^\lambda \frac{\epsilon_0 A^2}{2} \left[\sin^2(kz) + \cos^2(kz)\right] \, dz = \frac{\pi \epsilon_0 A^2}{k} \ . \tag{3.52}$$

Equating Eqs. (3.49) and (3.52) gives

$$\omega_A = 2.88 \gamma_L \ , \tag{3.53}$$

where we used Eq. (3.29) for the definition of $\gamma_L$. Note that the mode saturation is a bit low. It was expected to be $\omega_A = 3.2\gamma_L$, as previously mentioned.

Next, we add the contribution from the passing particles since their trajectories, see Fig. 3.1, are also affected by the interaction with the wave field, albeit less so than those of the trapped particles. We include their contribution by assuming that the saturated distribution can be expressed by simply averaging $F_0(v)$ over the particle trajectories, just as for the trapped particles. We can focus on the co-passing particles since the energy differences associated with the co- and counter-passing particles are equal. We compute the average of the distribution (3.46) for the co-passing particles,

$$F_{sat} = \frac{2}{\tau_+} \int_0^\lambda F_0 \frac{dz}{u} = C + \frac{2\lambda}{\tau_+} \left. \frac{dF_0}{du} \right|_{u=0} \ . \tag{3.54}$$

Here

$$\tau_+ = \int_0^{\tau_+} dt = 2 \int_0^\lambda \frac{dz}{u} \ , \tag{3.55}$$

is the time it takes a passing particle to pass two wavelengths, defined to match smoothly onto the bounce time for the trapped particles (3.37). By Eq. (3.35) this is calculated to be

$$\tau_+ = \frac{4}{\omega_A \kappa} K(1/\kappa) \ . \tag{3.56}$$

Note that, contrary to trapped particles, passing particles have $\kappa > 1$, where $\kappa$ is defined in (3.38). The contribution to the energy difference (3.45) between the initial and saturated state from the passing particles becomes

$$2\Delta E_+ = \frac{2 m_e \omega_{pe}}{k} \left. \frac{dF_0}{du} \right|_{u=0} \int_0^\lambda \int_{u_s}^\infty u \left[u - \frac{2\lambda}{\tau_+}\right] \, du \, dz \ , \tag{3.57}$$

which we calculate by a change in integration order to

$$2\Delta E_+ = \frac{2^6 e A \omega_{pe} \omega_A}{k^4} \left. \frac{dF_0}{du} \right|_{u=0} \int_1^\infty \left[E(1/\kappa) - \frac{\pi^2}{4} K^{-1}(1/\kappa)\right] \kappa^2 \, d\kappa \ . \tag{3.58}$$

Here,

$$E(k) = \int_0^{\pi/2} \sqrt{1 - k^2 \sin^2 \varphi}\, d\varphi \ , \tag{3.59}$$

is the *complete elliptical integral of the second kind* . The integral in (3.58) is calculated numerically and together with the contribution from the trapped particles (3.49) and the energy going into the wave (3.75), the balancing procedure gives a saturated wave amplitude at

$$\omega_A = 3.94\gamma_L \ . \tag{3.60}$$

This is reasonably close to the expected value of $\omega_A = 3.2\gamma_L$. The cause of the discrepancy is the assumption that the final saturated state is simply given by averaging the initial, linearly unstable distribution over the final state particle trajectories. The resulting distribution is therefore discontinuous at the separatrix of the saturated wave, whereas in reality there must be a transition layer that smoothly connects the inner and ambient averages. The width and shape of this layer can however only be found via dynamical, nonlinear analysis, so Eq. (3.60) represents the most refined result obtainable via energy balance arguments.

### 3.4.2 Dissipative Bump-on-Tail Model Near Marginal Stability

Weak dissipation is included in the background plasma, which reduces the effective linear growth rate to $\gamma_L - \gamma_d$ and gives an instability threshold $\gamma_d = \gamma_L$. Although natural first to investigate the effect of a small $\gamma_d$ general agreement is that experimental plasmas tend to support modes close to the instability threshold. For historical reasons we therefore consider the *near threshold regime* where $0 < \gamma_L - \gamma_d \ll \gamma_L, \gamma_d$. Note, though, that it does not have to be so. In fact, in Sec. 3.4.3 we mainly focus on the regime far from the instability threshold, where $\gamma_d \ll \gamma_L$.

The electric field amplitude evolution, when dissipation is present, is dependent on the rate and type of collisions and on the closeness to the stability threshold. Close to the threshold the presence of Krook-type [38] and velocity space diffusion [23] on the form (3.44) result in four regimes of possible mode amplitude evolution, cf. Fig. 3.6. If the collisionality is high enough, the mode amplitude saturates at a level that reflects the closeness to threshold, i.e the saturation amplitude depends on $\gamma_L - \gamma_d$. At somewhat lower collisionality, the saturation is followed by periodic modulations, and with even less collisions the modulations become chaotic. When the collision rate is very low or even non-existent it is difficult to immediately deduce what happens. We will come back later to this regime. For now we focus on the first three regimes.

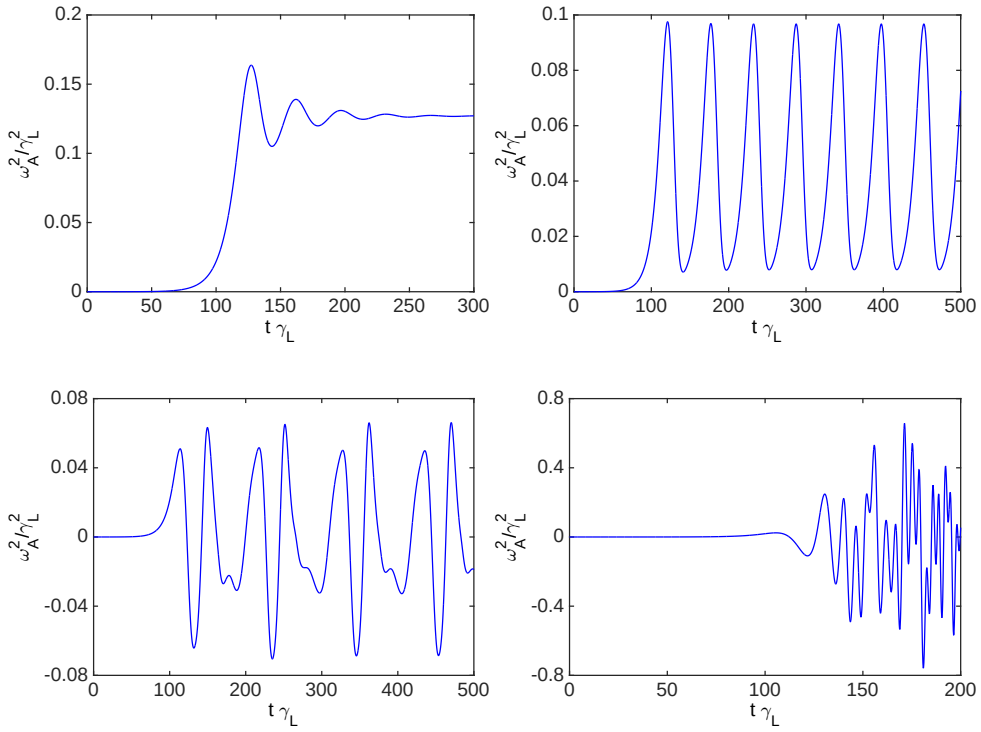


**Figure 3.6:** *Amplitude evolution near the instability threshold,* $\gamma_d/\gamma_L = 0.9$*, under the presence of Krook-type collisions of decresing rate,* $\beta/\gamma_L = 0.3$*,* $\beta/\gamma_L = 0.2$*,* $\beta/\gamma_L = 0.1$ *and* $\beta/\gamma_L = 0.01$*.*

The amplitude evolutions in Figs. 3.6a - c are only slightly nonlinear. This behavior can be captured by a perturbative approach where only the first order nonlinearity is included. An equation for the evolution of the wave amplitude takes the form [23]

$$\frac{dA}{d\tau} = A - \frac{1}{2}\int_0^{\tau/2} z^2 A(\tau - z) \int_0^{\tau-2z} e^{-\hat{\nu}^3 z^2(2z/3+x)-\hat{\beta}(2z+x)} A(\tau - z - x)A^*(\tau - 2z - x)\, dx\, dz \ , \quad (3.61)$$

where

$$A(\tau) \equiv \frac{\gamma_L^{1/2}}{(\gamma_L - \gamma_d)^{5/2}} \omega_A^2\left(t(\tau)\right) \ , \quad (3.62)$$

$$\hat{\nu} = \frac{\nu}{\gamma_L - \gamma_d} \ , \ \hat{\beta} = \frac{\beta}{\gamma_L - \gamma_d} \ , \quad (3.63)$$

$$\tau = (\gamma_L - \gamma_d)t \ , \quad (3.64)$$

and, $x$ and $z$ are dummy indices. As seen, the lowest order nonlinearity is cubic, and so Eq. (3.61) is often referred to as the cubic equation. Fig. 3.7 illustrates the solution to (3.61) in the near threshold regime and under the presence of Krook-type collisions of decreasing rate. As can be seen in Fig. 3.7d, when the collisionality is very low Eq. (3.61) is no longer accurate and full nonlinearity is required. This is the regime in Fig. 3.6d that we now further investigate in the collisionless limit.

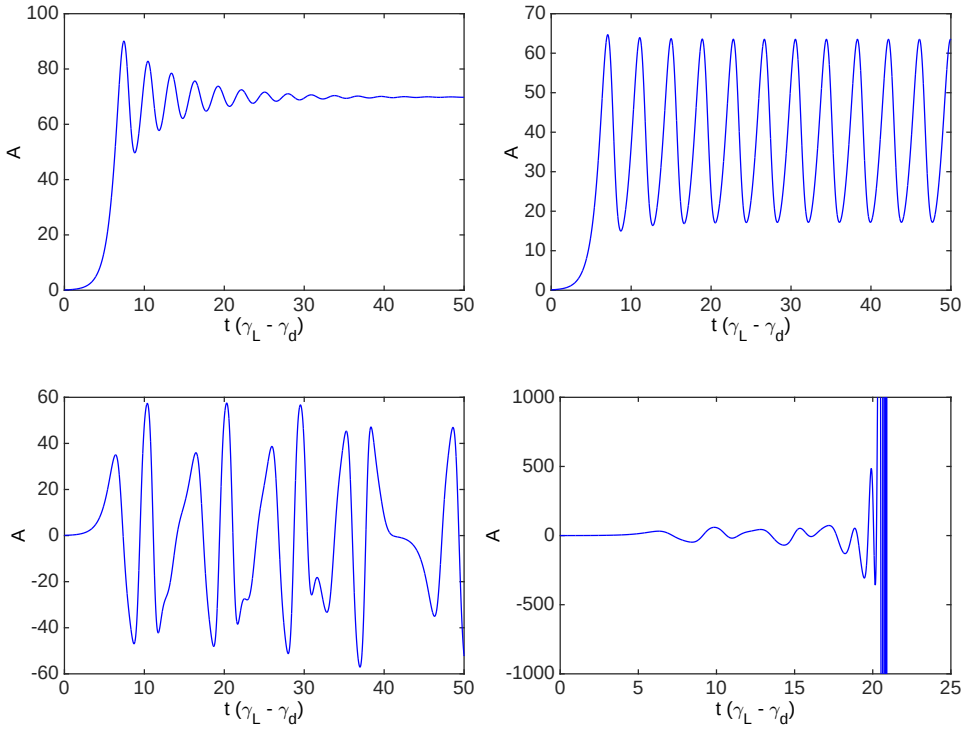


**Figure 3.7:** *Amplitude evolution near the instability threshold under the presence of Krook-type collisions of decresing rate,* $\beta/(\gamma_L - \gamma_d) = 5$, $\beta/(\gamma_L - \gamma_d) = 4$, $\beta/(\gamma_L - \gamma_d) = 2.5$ *and* $\beta/(\gamma_L - \gamma_d) = 2.3$. *The amplitude* $A$ *on the y-axis is normalized according to Eq.* (3.62).

Fig. 3.8 shows a phase space plot of the fast particle distribution at the wave-particle resonance near marginal stability in the collisionless limit. We observe the presence of coherent entities that emerge and move in phase space. Further studies of the distribution function in Figs. 3.9 and 3.10 reveil that the entities are regions of depletion/protrusion known as *holes* and *clumps*. There is a continuous production of holes and clumps that arise pairwise symmetrically shifted of the wave-particle resonance of the unstable bulk mode. Once formed, each pair traverse phase space in order to compensate for energy losses due to background dissipation. The convection of the holes is to

higher velocities and that of the clumps to lower velocities. To a first approximation the motion preserves the value of the distribution function for the trapped particles, i.e the level of the trapped particles remains constant, so the depth/height of the hole/clump relative to the ambient distribution increases as they move. Analytically, energy conservation between the power dissipated in the cold plasma and the energy gained by the motion of the holes and clumps results in a frequency shift that initially evolves according to $\omega - \omega_{pe} \propto \pm\sqrt{t}$ [39]. On a longer time scale fast particle collisions and other effects, such as the shape of the distribution, the dependence of $\gamma_d$ on the frequency, particle inclusion/release through the separatrix via amplitude growth/decrease etc. [40], can affect the frequency sweeping. The resulting spectrogram in Fig. 3.11 exhibits the frequency sweeping pattern. The shifts up and down of the side bands are synched to the motion of the holes and clumps in phase space.

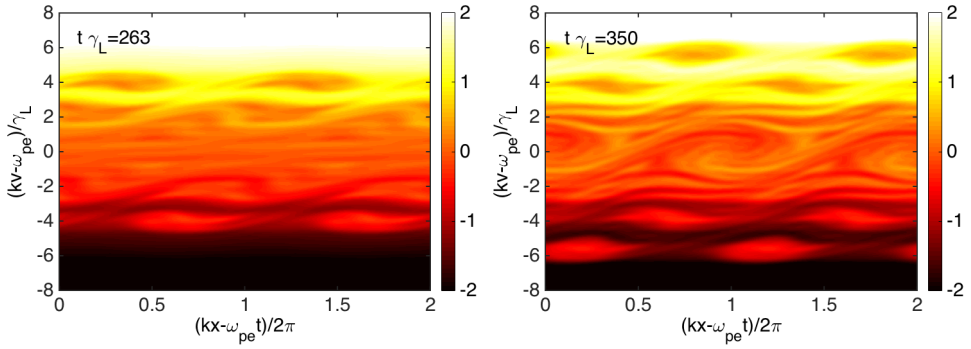


**Figure 3.8:** *Phase space plot of the fast particle distribution near marginal stability, $\gamma_d/\gamma_L = 0.9$, showing moving entities known as holes and clumps.*

Contrary to diffusive and Krook-type collisions, the inclusion of drag on the form (3.44) have been shown to promote the amplitude evolution regime in Fig. 3.6d. Furthermore, they introduce an asymmetry by enhancement of the holes and their sweeping rates and depletion of the clumps. Historically, this was first observed within the framework of Eq. (3.61) [35] where drag enters as a phase in the exponential that causes an oscillation of the nonlinear term that makes it impossible for the amplitude to saturate as opposed to the cases in Figs. 3.6a - c. The presence of drag has an interesting effect on the frequency sweeping pattern in the spectrogram, as can be observerd in Fig. 3.12 where so called hooks and steady state holes appear [34, 40]. Similar features have, in fact, been obseved experimentally [41]. This and other observed nonlinear mode evolutions in the different amplitude regimes will be the subject of Sec. 3.7.

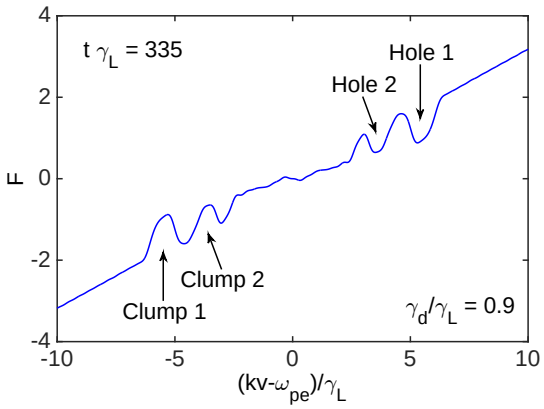


**Figure 3.9:** *Spatially averaged fast particle distribution in the near threshold regime. The figure displays the continuous production of hole-clump pairs that once formed will subsequently diverge far from the initial resonance.*

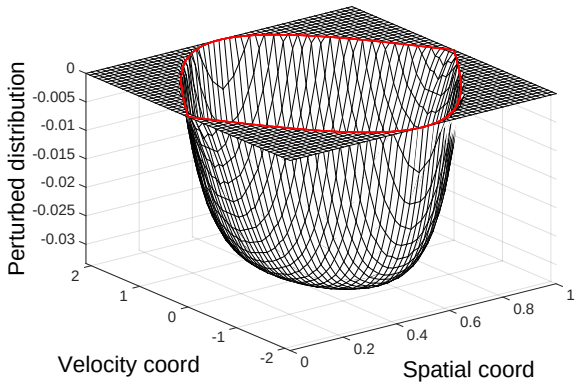


**Figure 3.10:** *A single hole as a trapping region in phase space with the separatrix highlighted in red [40]. Note that the distribution function on the y-axis is $\delta f = f - F_0$.*

### 3.4.3 Papers B and C: Dissipative Bump-on-Tail Model Far fom Marginal Stability

We now consider the effect of very weak dissipation, $\gamma_d/\gamma_L \ll 1$, which turns out to unlock the mysterious "spontaneous creation" [39] of the hole-clump formation mechanism. Fig. 3.13 shows a phase space time series of the fast particle distribution at the wave-particle resonance far from marginal stability in the collisionless limit. We observe the initial phase mixing of the resonant particles and the eye-shaped form of the saturated state. However, then dissipation kicks in and trapped particles are gradually released as the wave

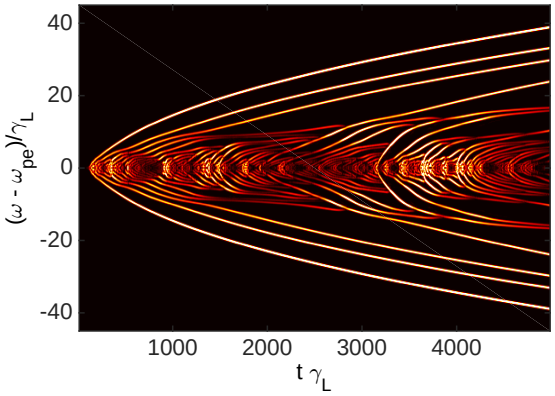


**Figure 3.11:** *Fourier spectrogram of the electric field amplitude showing frequency chirping near the stability threshold,* $\gamma_d/\gamma_L = 0.9$.

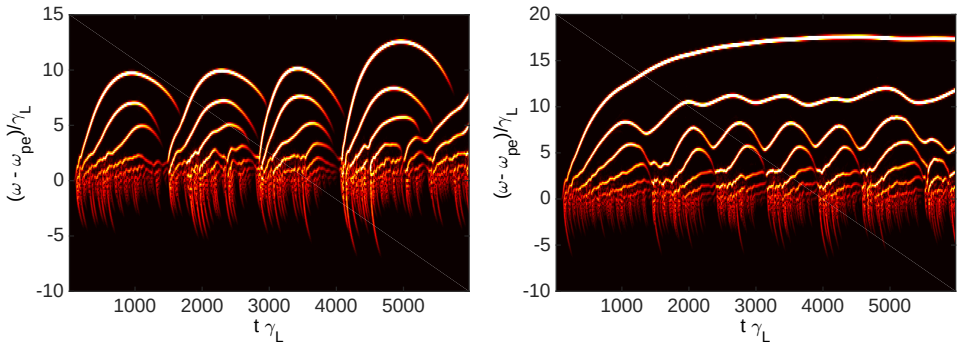


**Figure 3.12:** *Left: Spectrogram displaying hooked frequency sweeping. Right: Spectrogram showing a hole reaching a steady state frequency.*

amplitude damps out and the separatrix shrinks and the particles begin to stream freely. This generates a nearly unmodulated phase space plateau centered at the initial resonant velocity with a velocity width somewhat smaller than the maximum width of the separatrix. The initial mode eventually damps out but notice the presence of small up- and downshifted modulations just inside the edges of the plateau in the second snapshot. These begin to grow, as seen in the third snapshot, and eventually evolve into a hole-clump pair that detatches from the plateau. In the Fourier spectrogram they correspond to frequency sweeping modes and, as obseved in Fig. 3.14, the frequency sweeping is initiated noticeably shifted from the initial resonance.

In Papers B and C we follow and expand the disposition of [42] in order to substantiate the idea of the intermediate plateau as a hole-clump breeding ground via destabilization of *edge modes*. The edge modes are negative energy

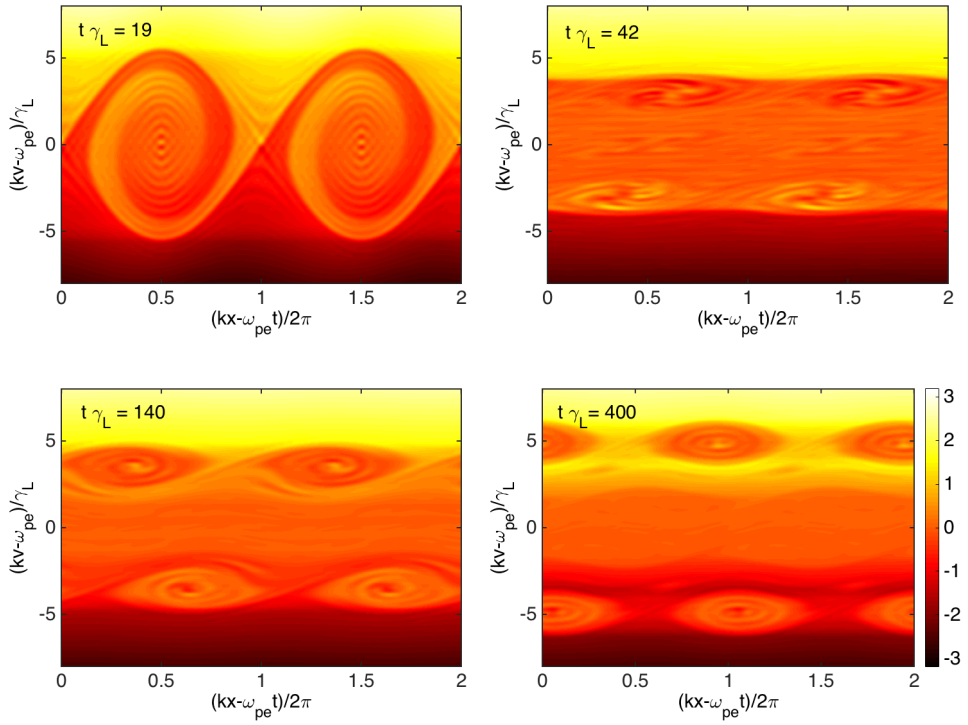


**Figure 3.13:** *Phase space plot of the fast particle distribution far from marginal stability,* $\gamma_d/\gamma_L = 0.1$.

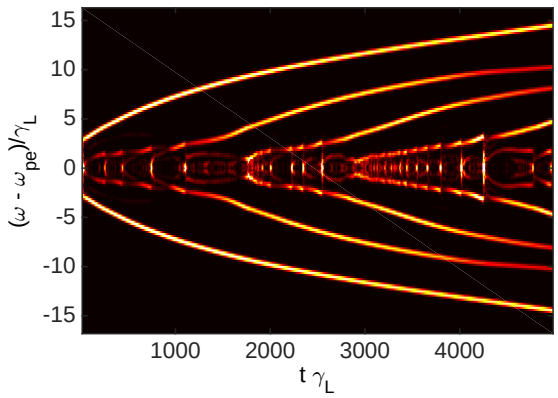


**Figure 3.14:** *Fourier spectrogram of the electric field amplitude showing frequency chirping far from the stability threshold,* $\gamma_d/\gamma_L = 0.1$.

eigenmodes of the plateau that grow in the presence of dissipation and nonlinearly evolve into holes and clumps, just as described in the previous paragraph. We employ linear and nonlinear stability analysis to investigate the role of fast

particle collisions and sources and also relaxation of the edge gradients of the plateau. It turns out that it is not the existence of a plateau that determines whether holes and clumps appear but rather the effect of collisions on that plateau. Krook-type collisions and velocity space diffusion inhibit hole-clump formation mainly by relaxation of the plateau that in turn reduces the growth rates of the edge modes in a fairly complicated way. The asymmetry of the growth rates of the holes and clumps, favoring the hole over the clump, in the presence of drag collisions is due to convection of the entire plateau down along the ambient slope distribution. Furthermore, slight relaxation of the edge gradients of the plateau is found to have no qualitative effect unless the corresponding Landau pole needs to be taken into account.

## 3.5 Negative Wave Energy

The reason that the edge modes of Papers B and C grow rather than damp in the presence of dissipation, and later develop into holes and clumps, is that they have negative wave energy. This was demonstrated in [42] via consideration of the so called dielectric energy [43, 44]

$$\mathcal{E}_D = \frac{\epsilon_0}{4}|A|^2\frac{\partial(\omega\epsilon_R)}{\partial\omega} \ . \tag{3.65}$$

Here, $A$ is the perturbed electric field amplitude, $\omega$ is the mode frequency and $\epsilon_R$ is the real part of the dispersion relation, fulfillling $\epsilon_R(\omega) = 0$. The dispersion relation according to Landau (cf. [45]) is

$$\epsilon = 1 - \frac{\omega_{pe}^2}{\omega(\omega + i2\gamma_d)} - \frac{\omega_{pe}^2}{kn_{e0}}\left[P\int_{-\infty}^{\infty}\frac{dF_P/dv}{\omega - kv}\,dv + i\pi\,\frac{dF_P}{dv}\bigg|_{v=\frac{\omega}{k}}\right] = 0 \ . \tag{3.66}$$

Under the assumptions that $k\Delta v, \gamma_d, \gamma_L \ll \omega_{pe}$ and $|\delta\omega| \leq k\Delta v$, where $\delta\omega \equiv \omega - \omega_{pe}$ and $F_P$ is the discontinuous "plateau" distribution in Fig. 3.15, we Taylor expand the second term and the dispersion relation takes the form

$$\epsilon_R = \delta\omega - \frac{\gamma_L}{\pi}\left[\ln(k\Delta v + \delta\omega) - \ln(k\Delta v - \delta\omega) + \frac{2\delta\omega k\Delta v}{(k\Delta v)^2 - \delta\omega^2}\right] = 0 \ . \tag{3.67}$$

To lowest order the condition for negative energy, i.e. $\mathcal{E}_D < 0$, becomes

$$\frac{k\Delta v}{\gamma_L}\left[1 - \left(\frac{\delta\omega}{k\Delta v}\right)^2\right]^2 < \frac{4}{\pi} \ , \tag{3.68}$$

which is indeed fulfilled for the edge modes.

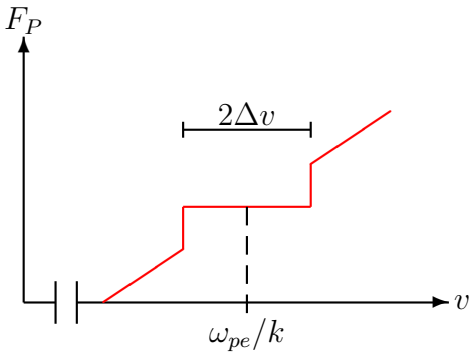


**Figure 3.15:** *Ideal shelf distribution with discontinuous edges.*

In order to meet initial criticism on the edge mode wave energy analysis presented above, a more rigorous expression for the wave energy is now derived following [46]. The distribution function is decomposed according to Eq. (3.7), which together with the Vlasov equation (3.8) allows us to express the perturbed electric field as

$$E = \frac{m_e}{e}\left(\frac{\partial \delta f}{\partial t} + v\frac{\partial \delta f}{\partial x}\right)\frac{1}{dF_0/dv} \ . \tag{3.69}$$

Note, there is no problem where $dF_0/dv = 0$ since by (3.10) $\delta f$ is then also zero. Now, Ampére's law relates the perturbed currents in the two electron species to the electric field

$$\frac{\partial E}{\partial t} = \frac{e}{\epsilon_0}\int_{-\infty}^{\infty}\sum_{\nu} v\,\delta f_\nu\, dv \ , \tag{3.70}$$

where $\nu$ indicates particle species, including bulk and energetic electrons. We multiply Eq. (3.70) with $E$, integrate over one period in space and get

$$\frac{1}{2}\int_0^\lambda \frac{\partial E^2}{\partial t}\, dx = \frac{e}{\epsilon_0}\int_0^\lambda\int_{-\infty}^{\infty}\sum_{\nu} v\delta f_\nu E\, dvdx \ , \tag{3.71}$$

which by (3.69) becomes

$$\frac{1}{2}\int_0^\lambda \frac{\partial E^2}{\partial t}\, dx = \frac{m_e}{\epsilon_0}\int_0^\lambda\int_{-\infty}^{\infty}\sum_{\nu} v\delta f_\nu\left(\frac{\partial \delta f_\nu}{\partial t} + v\frac{\partial \delta f_\nu}{\partial x}\right)\frac{dvdx}{dF_{0\nu}/dv} \ . \tag{3.72}$$

Since

$$\delta f\frac{\partial \delta f}{\partial x} = \frac{1}{2}\frac{\partial}{\partial x}(\delta f)^2 \ , \tag{3.73}$$

and due to periodicity in $\delta f$, the second term on the right hand side of (3.72) is zero. Thus, Eq. (3.72) can be expressed as

$$\frac{\partial}{\partial t}\left[\int_0^\lambda \left(-\frac{m_e}{2}\int_{-\infty}^{\infty}\sum_\nu \frac{v(\delta f_\nu)^2}{dF_{0\nu}/dv}dv + \frac{\epsilon_0}{2}E^2\right)dx\right] = 0 \ , \tag{3.74}$$

which defines the following constant,

$$\mathcal{E} = \int_0^\lambda \left(-\frac{m_e}{2}\int_{-\infty}^{\infty}\sum_\nu \frac{v(\delta f_\nu)^2}{dF_{0\nu}/dv}dv + \frac{\epsilon_0}{2}E^2\right)dx \ , \tag{3.75}$$

the *wave energy* in the electrostatic model.

We Fourier expand the perturbed quantities according to Eq. (3.9). However, Eq. (3.75) needs real quantities so we use

$$\mathrm{Re}\,[E] = A\cos(kx-\omega t) \ , \tag{3.76}$$

and, by (3.10),

$$\mathrm{Re}\,[\delta f_\nu] = -A\sin(kx-\omega t)\frac{e}{m_e}\frac{dF_{0\nu}/dv}{\omega - kv} \ . \tag{3.77}$$

For simplicity, we take the unperturbed distribution of the bulk electrons to be cold, $n_{e0}\delta(v)$, and for the energetic electrons we consider the discontinuous shelf distribution, i.e.

$$F_0(v) = n_{e0}\delta(v) + F_P(v) \ . \tag{3.78}$$

Eq. (3.75) becomes

$$\begin{aligned}\mathcal{E} &= \int_0^\lambda \left[\frac{n_{e0}e^2A^2}{2m_e\omega^2}\sin^2(kx-\omega t) + \frac{\epsilon_0 A^2}{2}\cos^2(kx-\omega t)\right]dx \\ &- \int_0^\lambda \frac{e^2A^2}{2m_e}\sin^2(kx-\omega t)\int_{-\infty}^{\infty} v\frac{dF_p/dv}{(\omega-kv)^2}\,dvdx \\ &= \frac{\lambda A^2}{4}\left[\frac{n_{e0}e^2}{m_e\omega^2} + \epsilon_0 - \frac{e^2}{m_e}\int_{-\infty}^{\infty} v\frac{dF_p/dv}{(\omega-kv)^2}\,dv\right] \ .\end{aligned} \tag{3.79}$$

In the end, what we need to calculate is

$$I = \int_{-\infty}^{\infty} v\frac{dF_p/dv}{(\omega-kv)^2}\,dv \ . \tag{3.80}$$

After a bit of algebra, we find

$$\begin{aligned}I = \frac{C}{k}\Big\{ &\ln(k\Delta v+\delta\omega) - \ln(k\Delta v-\delta\omega) \\ &+ \frac{2k\Delta v}{((k\Delta v)^2-\delta\omega^2)^2}\left[(k\Delta v)^2(3\delta\omega+2\omega_{pe}) - \delta\omega^3\right]\Big\} \ ,\end{aligned} \tag{3.81}$$

where

$$C \equiv \lim_{k\Delta v \to 0} \frac{dF_P}{dv}\bigg|_{v=\omega/k} = \frac{2kn_{e0}\gamma_L}{\pi\omega_{pe}^3} \tag{3.82}$$

is the gradient of the ambient, linear slope. We now express the logarithms of (3.81) using the dispersion relation (3.67). To the lowest order in $\delta\omega/\omega_{pe}$, i.e neglecting all $\delta\omega$ terms in the final term of Eq. (3.81), we then get back the condition (3.68).

## 3.6 Analytic Model for Smooth Relaxation of Plateau Edge

Nonlinear simulations in Paper B revealed that the rate of hole-clump production from a plateau distribution with smooth edges decreases and eventually ceases with increasing edge width. This was observed in the presence of velocity diffusion among the fast particles, which acts to relax the gradients of the distribution and thereby widen the edge region of the plateau, and when simulations were initiated with a continuous plateau distribution of varying edge width. In Paper B, we surmised that this was due to Landau damping from a nonzero gradient of the distribution at the location of the edge modes. For that reason we now study the distribution function

$$F_P(u) = Cu\left\{1 - \frac{1}{2}\left[\tanh\left(\frac{u+\Delta u}{a}\right) - \tanh\left(\frac{u-\Delta u}{a}\right)\right]\right\} , \tag{3.83}$$

used in Paper B and depicted in Fig. 3.16. Here, $u$ is the wave frame velocity (3.33), $C$ is given by (3.82) and $a$ sets the extent of the edge region. In the limit $a \to 0$, Eq. (3.83) reduces to the discontinuous shelf distribution in Paper B.

The dispersion relation (3.66) is, just as in the previous section, Taylor expanded and simplifies to

$$\delta\omega + i\gamma_d - \frac{\gamma_L}{\pi}\left[P\int_{-\infty}^{\infty}\frac{1}{C}\frac{dF_P/du}{u-\delta\omega}\,du + i\pi\,\frac{1}{C}\frac{dF_P}{du}\bigg|_{u=\delta\omega}\right] = 0 . \tag{3.84}$$

We introduce the dimensionless variables

$$z \equiv \frac{\delta\omega}{\Delta u} , \quad \alpha \equiv \frac{a}{\Delta u} , \quad x \equiv \frac{u}{\Delta u} , \quad \gamma \equiv \frac{\gamma_d}{\gamma_L} , \quad w \equiv \frac{\pi\Delta u}{\gamma_L} , \tag{3.85}$$

and consider marginal stability, at which $z \in \mathbb{R}$, contrary to the unstable situation described in Papers B and C. Then the first and third terms in (3.84) balance individually, as do the second and fourth terms (i.e the dissipative

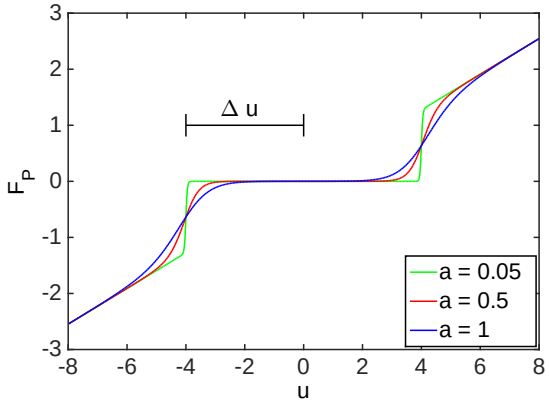


**Figure 3.16:** *Simplified fast electron plateau distribution with smooth edges used in Paper B.*

term, which acts to excite the edge modes, and the Landau term, which will be shown to damp them). So, we get

$$wz = P\int_{-\infty}^{\infty}\left\{1-\frac{1}{2}\left[\tanh\left(\frac{x+1}{\alpha}\right)-\tanh\left(\frac{x-1}{\alpha}\right)\right]\right.$$
$$\left.+\frac{x}{2\alpha}\left[\tanh^2\left(\frac{x+1}{\alpha}\right)-\tanh^2\left(\frac{x-1}{\alpha}\right)\right]\right\}\frac{dx}{x-z}\ , \tag{3.86a}$$

and

$$\gamma = 1-\frac{1}{2}\left[\tanh\left(\frac{z+1}{\alpha}\right)-\tanh\left(\frac{z-1}{\alpha}\right)\right]$$
$$+\frac{z}{2\alpha}\left[\tanh^2\left(\frac{z+1}{\alpha}\right)-\tanh^2\left(\frac{z-1}{\alpha}\right)\right]\ . \tag{3.86b}$$

The contribution from the first term in the integral in (3.86a) is zero, but the other terms require numerical treatment. We first note that the remaining integrands are negligably small outside large enough $|x|$, say, $|x| = s$, which allows us to limit the evaluation of the integrals to the interval $[-s, s]$. We calculate the principal value by adding and subtracting certain terms, which results in a finite value of the integral in (3.86a) in the limit $x \to z$ so that numerical integration can be employed without problems. Eq. (3.86a) becomes

$$wz = I_2 + I_3\ , \tag{3.87}$$

where

$$I_2 = \int_{-s}^{s} \Bigg\{ -\frac{1}{2}\left[\tanh\left(\frac{x+1}{\alpha}\right) - \tanh\left(\frac{x-1}{\alpha}\right)\right] + \frac{1}{2}\left[\tanh\left(\frac{z+1}{\alpha}\right) - \tanh\left(\frac{z-1}{\alpha}\right)\right] \Bigg\} \frac{dx}{x-z} - \frac{1}{2}\left[\tanh\left(\frac{z+1}{\alpha}\right) - \tanh\left(\frac{z-1}{\alpha}\right)\right] \ln\left|\frac{s-z}{-s-z}\right| , \tag{3.88a}$$

and

$$I_3 = \int_{-s}^{s} \Bigg\{ \frac{1}{2\alpha}\left[\tanh^2\left(\frac{x+1}{\alpha}\right) - \tanh^2\left(\frac{x-1}{\alpha}\right)\right] - \frac{1}{2\alpha}\left[\tanh^2\left(\frac{z+1}{\alpha}\right) - \tanh^2\left(\frac{z-1}{\alpha}\right)\right] \Bigg\} \frac{x}{x-z} dx + \frac{1}{2\alpha}\left[\tanh^2\left(\frac{z+1}{\alpha}\right) - \tanh^2\left(\frac{z-1}{\alpha}\right)\right] \left[z \ln\left|\frac{s-z}{-s-z}\right| + 2s\right] . \tag{3.88b}$$

Once $z$ has been calculated via Eq. (3.87), the marginal stability criterion for $a(w)$ is calculated from (3.86b), displayed in Fig. 3.17 and verified using nonlinear simulations of the initiated plateau in Eq. (3.83) when $\gamma = 0.1$, $\gamma = 0.2$ and $\gamma = 0.5$ at $w = 4\pi$. The conclusion of this analysis is that, unlike for positive energy waves, the positive slope of the fast particle distribution at the plateau edge acts to damp edge modes, much like ordinary Landau damping. The analytical results match perfectly onto the nonlinear numerics, as demonstrated by considering marginal stability.

## 3.7 Connection to Fast Particle Driven Instabilities in Tokamak Plasmas

Similarly as in previous sections, we consider resonant interaction between a low density population of energetic ions and a TAE. Only now, in the more complicated three dimensional geometry of a tokamak, the wave phase velocity needs to be synched with the poloidal and toroidal orbital frequencies of the energetic particles or multiples thereof, cf. Sec. 2.3.4. Furthermore, as previously mentioned, the linear instability growth rate depends on the gradient of the fast particle pressure. A commonly accepted idea is therefore that a gradual build-up of the energetic ion population, due to auxiliary heating or nuclear fusion reactions, eventually leads to a positive linear growth rate and mode destabilization. The energetic ions subsequently loose energy to the wave,

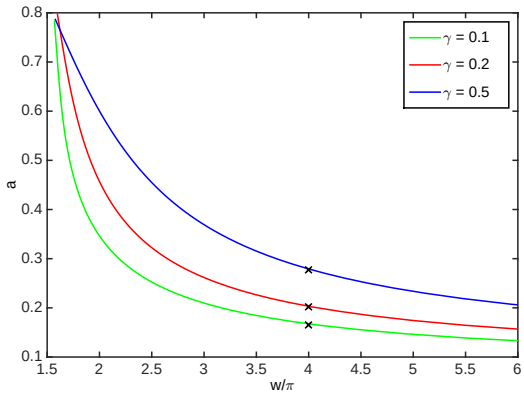


**Figure 3.17:** *Edge width parameter a(w) corresponding to marginal stability when* $\gamma = 0.1$*,* $\gamma = 0.2$ *and* $\gamma = 0.5$*. Result of nonlinear simulations at* $w = 4\pi$ *are shown for the three values of* $\gamma$*.*

which relaxes the gradient of the distribution toward a critical slope. This sequence of gradual build up followed by a collapse is expected to maintain the gradient just above critical level, i.e in the near threshold regime, and, historically, this idea has been supported by experimental results, cf. [8]. Recently, however, observations of bursting TAEs on the ASDEX Upgrade indicate that mode destabilization may occur far from the stability threshold [47].

Experimentally, there have been many observations where the nonlinear mode evolution matches those of the numerically calculated amplitude evolutions in Fig. 3.6. The first three scenarios are illustrated in Fig. 3.18, where, on JET, ICRH accelerated ions excite TAEs of different toroidal mode number. As the ICRH power is increased the initially saturated amplitude exhibit modulations and the Fourier signal splits (this phenomenon is known as *frequency splitting*), and finally blurrs out as the wave evolution becomes chaotic. In relation to the bump-on-tail model, the transition from steady state to modulations of the mode amplitude occurs due to a gradual build up of the linear growth rate as the fast particle pressure builds up. The diffusive collisionality is meanwhile constant, which in turn leads to an effective decrease in collision rate [48]. A Doppler shift, due to plasma rotation from unidirectional NBI beams, separates the modes in frequency. The final mode evolution in Fig. 3.6, which leads to frequency sweeping signals (see Fig. 3.19), is mainly found on the spherical tokamak MAST, where the TAEs are excited by NBI generated fast ions, although, hooked frequency sweeping events have also been observed on JET [41].

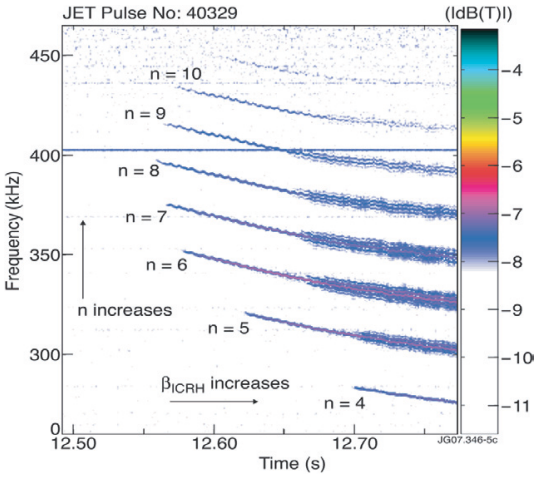


**Figure 3.18:** *Magnetic spectrogram of JET shot #40329 as presented in [8] displays ICHR driven Alfven instabilities with toroidal mode numbers, which range from $n = 4$ to $n = 10$.*

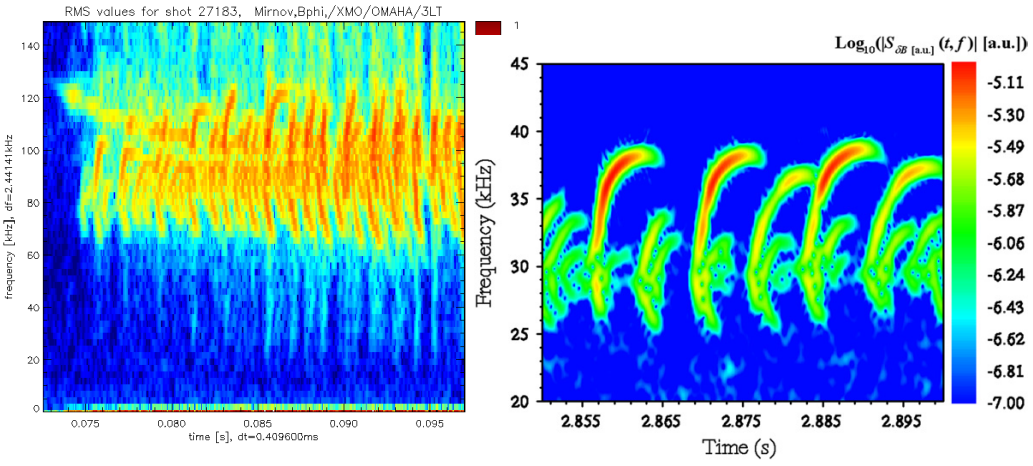


**Figure 3.19:** *Magnetic spectrogram of MAST shot #27183 (left), displaying frequency sweeping TAEs and of JET shot #54895 (right), displaying hooked frequency sweeping.*

# Bibliography


[1] U. S. Energy Information Administration, *www.eia.doe.gov*, Jan 4, 2016.

[2] J. Wesson, *Tokamaks*, Oxford University Press, Oxford, 3rd edition (2004).

[3] CCFE Culham Center Fusion Energy, *www.ccfe.ac.uk*, Jan 26, 2016.

[4] International Thermonuclear Experimental Reactor, *www.ITER.org*, Jan 4, 2016.

[5] J. D. Lawson, *Some Criteria for a Power Producing Thermonuclear Reactor*, Phys. Soc. B **70**, 6 (1957).

[6] A. Fasoli, C. Gormenzano, H. L. Berk, B. . Breizman, S. Briguglio, D. S. Darrow, N. . Gorelenkov, W. W. Heidbrink, A. Juan, S. V. Konovalov, R. azikian, J. M.oterdaeme, S. E. Sharapov, D. Testa, K. Tobita, Y. Todo, G. Vlad and F. Zonca, *Progress in the ITER Physics Basis, Chapter 5: Physics of energetic ions*, Nucl. Fusion **47**, S264 (2007).

[7] W. W. Heidbrink and G. J. Sadler, *The Behavior of Fast Ions in Tokamak Experiments*, Nucl. Fusion **34** (4), 535 (1994).

[8] S. E. Sharapov, B. Alper, H. L. Berk, D. N. Borba, B. N. Breizman, C. D. Challis, I. G. J. Classen, E. M. Edlund, J. Eriksson, A. Fasoli, E. D. Fredrickson, G. Y. Fu, M. Garcia-Munoz, T. Gassner, K. Ghantous, V. Goloborodko, N. N. Gorelenkov, M. P. Gryaznevich, S. Hacquin, W. W. Heidbrink, C. Hellesen, V. G. Kiptily, G. J. Kramer, P. Lauber, M. K. Lilley, M. Lisak, F. Nabais, R. Nazikan, R. Nyqvist, M. Osakabe, C. Perez von Thun, S. D. Pinches, M. Podesta, M. Porkolab, K. Shinohara, K. Schoepf, Y. Toda, K. Toi, M. A. Van Zeeland, I. Voitsekhovich, R. B. White, V. Yavorskij, ITPA EP TG and JET-EFDA contributors *Energetic particle instabilities in fusion plasmas*, Nucl. Fusion **53**, 104022 (2013)

[9] J. P. Freidberg, *Ideal magnetohydrodynamic theory of magnetic fusion systems*, Rev. Mod. Phys. **54** (3), 801 (1982).

[10] H. Goldstein, C. Pool, J. Safko, *Classical Mechanics*, 3Addison Wesley, 3rd edition (2002).

[11] M. Lisak, *On the Linear and Quasi-Linear Theory of Thermonuclear Instabilities in a Tokamak Reactor*, Phys. Scripta **29** (1), 87 (1984).

[12] J. Candy, B. N. Breizman, J. W. Van Dam and T. Ozeki, *Multiplicity of low-shear toroidal Alfvén eigenmodes*, Phys. Lett. A **215**, 299 (1996).

[13] M. N. Rosenbluth, H. L. Berk, J. W. Van Dam and D. M. Lindberg, *Mode structure and continuum damping of high-n toroidal Alfvén eigenmodes*, Phys. Fluids B **4** (7), 2189 (1992).

[14] H. L. Berk, J. W. Van Dam, Z. Guo and D. M. Lindberg, *Continuum damping of low-n toroidicity induced shear Alfvén eigenmodes*, Phys. Fluids B **4** (7), 1806 (1992).

[15] L. Chen and A. Hasegawa, *Plasma heating by spatial resonance of Alfvén wave*, Phys. Fluids **17** (7), 1399 (1974).

[16] C. Z. Cheng, L. Chen and M. S. Chance, *High-n Ideal and Resistive Shear Alfvén Waves in Tokamaks*, Ann. Phys. **161**, 21 (1985).

[17] G. T. A. Huysmans, J. P. Goedbloed and W. O. K. Kerner, p. 371 in *Proc. of the CP90 Conference on Computational Physics, Amsterdam*, World Scientific, Singapore, 1991.

[18] B. N. Breizman and S. E. Sharapov, *Energetic particle drive for toroidicity-induced Alfvén eigenmodes and kinetic toroidicity-induced Alfvén eigenmodes in a low-shear tokamak*, Plasma Phys. Control. Fusion **37**, 1057 (1995).

[19] A. B. Mikhailovskii, G. T. A. Huysmans, W. O. K. Kerner and S. E. Sharapov, *Optimization of Computational MHD Normal-Mode Analysis for Tokamaks*, Plasma Phys. Rep. **23** (10), 844 (1997)

[20] T. Fülöp, M. Lisak, Ya I Kolesnichenko, D. Andersson, *Finite orbit width stabilizing effect on toroidal Alfvén eigenmodes excited by passing and trapped energetic ions*, Plasma Phys. Control. Fusion **38** (1996).

[21] S. E. Sharapov, *Fast Particle Driven Alfvén Eigenmodes in Tokamaks*, Fusion Science and Technology **57** 156 (2010).

[22] G. Y. Fu and J. W. Van Dam, *Excitation of the toroidicity-induced shear Alfvén eigenmode by fusion alpha particles in an ignited tokamak*, Phys. Fluids B **1** (10), 1949 (1989).

[23] B. N. Breizman, H. L. Berk, M. S. Pekker, F. Porcelli, G. V. Stupakov and K. L. Wong, *Critical nonlinear phenomena for kinetic instabilities near threshold*, Phys. Plasmas **4**(5), 1559 (1997).

[24] W. W. Heidbrink, E. D. Fredrickson, T. K. Mau, C. C. Petty, R. I. Pinsker, M. Porkolab and B. W. Rice, *High harmonic ion cyclotron heating in DIII-D: Beam ion absorption and sawtooth stabilization* Nucl. Fusion **39** 1369 (1999).

[25] M. K. Lilley and B. N. Breizman, *Convective transport of fast particles in dissipative plasmas near an instability threshold* Nucl. Fusion **52** 094002 (2012).

[26] B. V. Chirikov , *A universal instability of many-dimensional oscillator systems* Phys. Rep **52** No. 5 (1979)

[27] D. A. Gurnett and A. Bhattacharjee *Introduction to plasma physics with space and laboratory applications* Cambridge University Press 2005.

[28] L. D. Landau, *On the vibrations of the electronic plasma*, J. Physics **10**, 25 (1946).

[29] G. Arfken, H. Weber, F. Harris, *Mathematical methods for physicists*, Academic Press, Oxford, 7th edition (2013).

[30] R. Betti and J. P. Freidberg, *Stability of Alfvén gap modes in burning plasmas*, Phys. Fluids B **4** (6), 1465 (1992).

[31] N. N. Gorelenkov and S. E. Sharapov, *On the collisional damping of TAE-modes on trapped electrons in tokamaks*, Phys. Scripta **45**, 163 (1992).

[32] M. N. Rosenbluth, H. L. Berk, J. W. Van Dam and D. M. Lindberg, *Continuum damping of high-mode-number toroidal Alfvén waves*, Phys. Rev. Lett. **68** (5), 596 (1992).

[33] R. M. Nyqvist and S. E. Sharapov, *Asymmetric radiative damping of low shear toroidal Alfvén eigenmodes*, Phys. Plasmas **19**, 082517 (2012).

[34] M. K. Lilley, B. N. Breizman and S. E. Sharapov, *Effect of dynamical friction on nonlinear energetic particle modes*, Phys. Plasmas **17**, 092305 (2010).

[35] M. K. Lilley, B. N. Breizman and S. E. Sharapov, *Destabilizing effect of dynamical friction on fast-particle-driven waves in a near-threshold nonlinear regime*, Phys. Rev. Lett. **102**, 195003 (2009).

[36] M. K. Lilley (2010), source code available from https://github.com/mklilley/BOT

[37] See National Technical Information Service Document No. AD730123 PGG-93, B. Fried, C. Lui, W. Means and R. Sagdeev, University of California Report No. AD730123 PGG-93, 1971. Copies may be ordered from the National Technical Information Service, Springfield, Virginia 22161.

[38] H. L. Berk, B. N. Breizman and M. S. Pekker, *Nonlinear dynamics of a driven mode near marginal stability*, Phys. Rev. Lett. **76** (8) 1256, (1996).

[39] H. L. Berk, B. N. Breizman and N. V. Petviashvili, *Spontaneous hole-clump pair creation in weakly unstable plasmas*, Phys. Lett. A **234** 213 (1997).

[40] R. M. Nyqvist and B. N. Breizman, *Modeling of long range frequency sweeping for energetic particle modes*, Phys. Plasmas **20**, 042106 (2013).

[41] H. L. Berk, C. J. Boswell, D. Borba, A. C. A. Figueiredo, T. Johnson, M. F. F. Nave, S. D. Pinches, S. E. Sharapov and JET-EFDA Contributors, *Explanation of the JET n = 0 chirping mode*, Nucl. Fusion **46**, S888 (2006).

[42] M. K. Lilley and R. M. Nyqvist, *Formation of phase space holes and clumps*, Phys. Rev. Lett. **112**, 155002 (2014).

[43] P. L. Auer, H. Hurwitz and R. D. Miller, *Collective oscillations in a cold plasma*, Phys. Fluids **1** 501 (1958).

[44] L. Brillouin, *Wave propagation and group velocity*, Academic New York (1960).

[45] L. D. Landau, *On the vibrations of the electronic plasma*, J. Physics **10**, 25 (1946).

[46] P. J. Morrison, *Dielectric energy versus plasma energy, and Hamiltonian action-angle variables for the Vlasov equation*, Phys. Fluids B **4**, 10 (1992).

[47] P. Lauber, M. Schneller, X. Wang, A. Biancalani, D. Zarzoso, T. Hayward, G. Papp, B. D. Scott, S. D. Pinches, S. Sharapov, M. Maraschek, B. Geiger, V. Nikolaeva, L. Guimares, A. Mlynek, I. Classen, V. Igochine, A. Gude and C. Hopf, *Kinetic models for energetic particle physics in tokamaks - verifications, validation and predictions for ITER* Theory of Fusion Plasmas: Joint Varenna-Lausanne International Workshop, Villa Monastero, Varenna, Italy, September 1 – 5, 2014.

[48] W. Kerner, D. Borba, S. E. Sharapov, B. N. Breizman, J. Candy, A. Fasoli, L. C. Appel, R. Heeter, L. G. Eriksson and M. J. Mantsinen, *Theory of Alfvén eigenmode instabilities and related alpha particle transport in JET deuterium-tritium plasmas*, Nucl. Fusion **38** 9 (1998).

# Paper A

# Paper B

# Paper C